Low-Gravity Combustion Synthesis: Theoretical Analysis of Experimental Evidences

A. M. Locci, R. Licheri, R. Orrù, A. Cincotti and G. Cao
Dipartimento di Ingegneria Chimica e Materiali, Centro Studi sulle Reazioni Autopropaganti (CESRA), Unità di Ricerca del Consorzio Interuniversitario Nazionale per la Scienza e Tecnologia dei Materiali (INSTM), Università degli Studi di Cagliari, Piazza d'Armi 109123, Cagliari, Italy

J. De Wilde, F. Lemoisson and L. Froyen
Dept. MTM, K.U. Leuven, Kasteelpark Arenberg 44, B-3001 Heverlee, Belgium

I. A. Beloki
INASMET, Parque Tecnologico E-20009 Donostia - San Sebastian, Spain;

A. E. Sytschev and A. S. Rogachev
Institute of Structural Macrokinetics and Materials Science, Russian Academy of Sciences, Chernogolovka, Moscow Region, 142432 Russia

D. J. Jarvis
European Space Agency, Keplerlaan 1 - P.O Box 299 - 2200 Ag Noordwijk Zh - The Netherlands

DOI 10.1002/aic.11006
Published online October 4, 2006 in Wiley InterScience (www.interscience.wiley.com).

The results obtained during a parabolic flight campaign sponsored by ESA on March 2002, and related to the combustion synthesis of TiB_2 − x$TiAl$ and TiB_2 − x$TiAl_3$ composites are reported. Besides classical SHS experiments performed using cylindrical pellets, combustion front quenching experiments using conical samples placed inside a copper block are also conducted. Similar experiments are carried out under terrestrial conditions, for the sake of comparison. As expected, under both low-gravity and terrestrial conditions, it is found that combustion temperature and front propagation velocity decrease as the system exothermicity is reduced, that is, when the aluminide/diboride molar ratio is augmented. However, it is observed that reaction front propagates relatively slower under low-gravity conditions. Consistently, the extinction of the combustion front occurs earlier when the reaction is performed under reduced gravity conditions. A theoretical analysis performed by means of appropriate dimensionless numbers is proposed to provide possible explanations of the main experimental evidences reported in the literature on this subject, including those shown in this work. Specifically, this analysis reveals that the relatively higher-propagation velocity observed under terrestrial conditions may be due to the correspondingly lower-sample porosity change, which in turn limits the thermal conductivity decreasing in the reaction zone. In addition, free convection phenomena taking place in the molten phase formed at the reaction zone are able to justify the difference in combustion wave velocity experimentally observed under terrestrial conditions between top and bottom ignition configurations. Moreover, it is found that finer microstructure typically observed under low-gravity is likely a consequence of the reduced coalescence phenomena taking place in such conditions. © 2006 American Institute of Chemical Engineers *AIChE J,* 52: 3744–3761, 2006

Keywords: combustion synthesis, microgravity, heat transfer, mass transfer, dimensional analysis

G. Cao is also affiliated with CRS4, Parco Scientifico e Tecnologico, POLARIS, Edificio 1, 09010 Pula (CA), Italy
Correspondence concerning this article should be addressed to G. Cao at cao@dicm.unica.it or R. Orrù at orru@visnu.chem.unica.it.

Introduction

Self-propagating high-temperature reactions are characterized by the fact that, once ignited by an external energy source, they are able to propagate in the form of a combustion wave through the reacting mixture without requiring additional energy. This type of reaction has been exploited to establish the technique referred to in the literature with the acronym of self-propagating high-temperature synthesis (SHS). The latter permits to obtain a variety of advanced materials, such as ceramics, intermetallics, composites, solid solutions, functionally graded materials, and so on.[1-5] The SHS method, also known as combustion synthesis, has received attention for its simplicity, short reaction time, easy-to-build equipment, low energy requirements, and possibility of obtaining complex or metastable phases.

It is well known that several parameters affect combustion synthesis reactions. For instance, reaction stoichiometry, green density, reactants-particle size, heating and cooling rates, as well as the presence of a gravitational field, are demonstrated to have an important effect on final product morphology and properties. Specifically, stoichiometry (including the use of inert components) affects the exothermicity of synthesis reaction and, therefore, the dynamics of the combustion process. In particular, the addition of inert components leads to heat subtraction, and, consequently, to a decrease of combustion temperature. The green density of the reacting sample also influences SHS processes, since it affects system reactivity, as well as thermal conductivity of the compact.

Similar considerations can be made for other operating parameters. In addition, gravity has been shown to play an important and specific role in self-propagating high-temperature synthesis reactions.[6-24] In fact, combustion synthesis and related structure formation mechanisms involve several stages including melting of reactants and products, spreading of the melt, droplets coalescence, diffusion and convection, buoyancy of solid particles, and solidification of liquid products, most of which are affected by gravity. In particular, generated liquid and gaseous species will be subject to gravity-driven fluid flow and gas transport and convection, which are likely to significantly affect both SHS reaction stability, and morphology of product phases. It is then apparent the importance of investigating the effect of gravity on the aforementioned phenomena to identify the detailed mechanism of reaction evolution and structure formation. Specifically, low-gravity experiments are able to permit the general mechanism of combustion and structure formation to be revealed without the disturbing effect of gravity, as well as by performing a direct comparison to data obtained from equivalent ground based experiment.

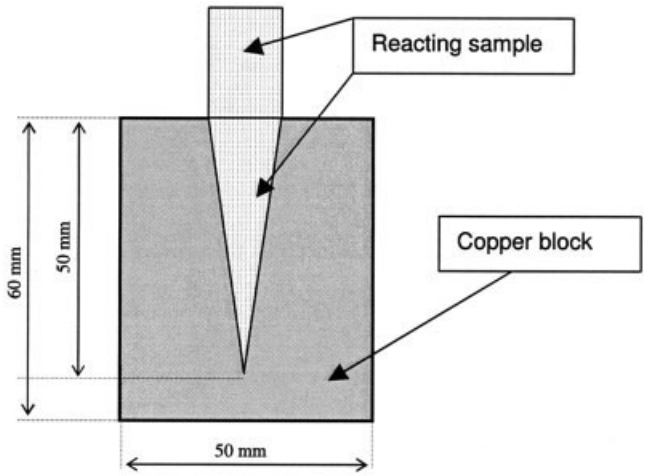

Figure 1. Cylindrical and conical sample configuration used for mechanistic investigation.

Table 1. Characteristics of Reactant Powders

Reactants	Powders Size	Purity	Vendor
Ti	$<20\ \mu m$	99.7%	Atlantic Equipment Engineering [Cat. No. TI-101]
Al	-200 mesh	99%	Aldrich [Cat. No. 214752]
Amorphous B	—	95–97%	Fluka [Cat. No. 15580]

Along these lines, interesting results have been recently obtained in USA, Japan, Canada, Europe, and Russia. It has been shown that products with finer and more uniform microstructure are typically obtained under low-gravity conditions with respect to terrestrial ones.[10,11,21,24]

The main experimental results related to the synthesis of the composites TiB_2-xTiAl and TiB_2-xTiAl$_3$, under both terrestrial and low-gravity (10^{-2} g where g is the terrestrial gravity acceleration) conditions are first reported in this work. Experiments under low-gravity conditions have been performed during the 32nd ESA Parabolic Flights Campaign (Bordeaux, March 2002).

Subsequently, the obtained results along with the most significant experimental evidence on this field reported in the literature, are discussed by taking advantage of a recently proposed theoretical approach.[25] A thorough analysis of gravity effects on combustion synthesis process has been performed.

Experimental Setup and Methods

The starting mixtures were prepared by mixing the elemental reactants, whose properties are reported in Table 1, according to the following reactions

$$(1 + x)\mathrm{Ti} + 2\mathrm{B} + 3x\mathrm{Al} \rightarrow \mathrm{TiB_2} - x\mathrm{TiAl_3} \quad (1)$$

$$(1 + x)\mathrm{Ti} + 2\mathrm{B} + x\mathrm{Al} \rightarrow \mathrm{TiB_2} - x\mathrm{TiAl} \quad (2)$$

where the molar ratio x was varied in the range 1–3 and 2–4 for reaction Eqs. 1 and 2, respectively.

Cylindrical pellets (16 mm dia. and 20 mm high) were used for combustion synthesis experiments. In addition, combustion front quenching (CFQ) experiments were also conducted by pressing the starting mixture into a conical shaped cut in a copper block until the desired density (about 55% of the theoretical value) is reached. The configuration used is represented in Figure 1.

The combustion reaction is then initiated at the top of the sample by means of a tungsten coil (mod. H2-040, R.D. Mathis Company) connected to a power supply. For the case of CFQ runs, the combustion wave travels toward the apex of the wedge, and is extinguished due to the combination of intense heat removal by the copper block, and the shrinkage of the cross-section. Simultaneously, intermediate and final products

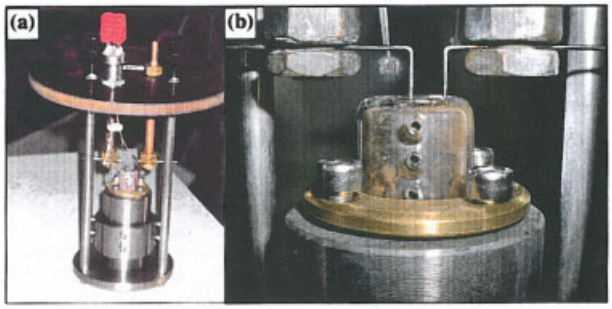

Figure 2. General (a), and detailed (b) views of sample holder used during parabolic flights.

[Color figure can be viewed in the online issue, which is available at www.interscience.wiley.com.]

are frozen and the evolution of the structure during preheating, combustion and post-combustion, may be followed by studying product microstructure and composition at different areas relative to the location where the combustion front is extinguished.

Either for the case of cylindrical pellets or during CFQ experiments, temperature evolution as well as average velocity of combustion wave were measured using thermocouples (C-type, 127 μm dia., Omega Engineering, Inc.) embedded in the pellet. Specifically, the average values of front velocity were determined from the temperature-time profiles of different thermocouples inserted in the pellet at known axial distances.

Sample stability during low-gravity experiments was guaranteed by means of a quartz tube properly connected to the copper block, in the case of CFQ experiments or to a steel cylindrical support for classical SHS samples. As an example, Figure 2a–b show two images of the sample holder considered during CFQ experiments.

The experimental apparatus used for parabolic flights experiments (cf. Figure 3) consists of a reaction chamber, an argon tank, an energy source required for reaction ignition, a vacuum pump, and a holding box where the sample holders, to be sequentially loaded to the reaction chamber, are placed. In addition, a video camera and a computer system equipped with

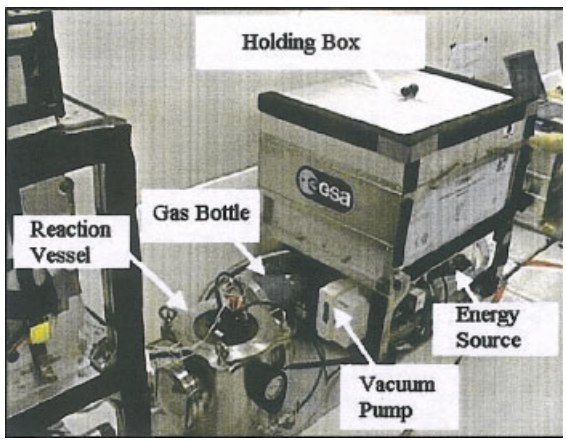

Figure 3. Experimental setup used for SHS under low-gravity conditions.

[Color figure can be viewed in the online issue, which is available at www.interscience.wiley.com.]

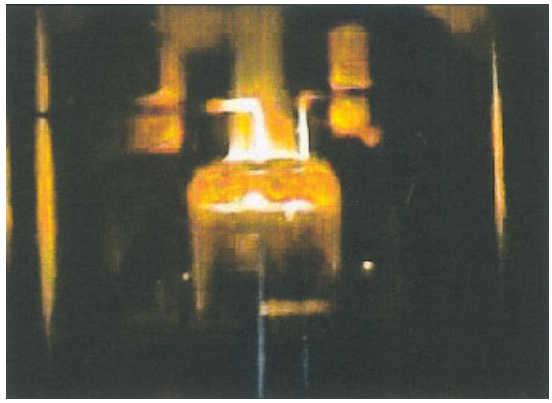

Figure 4. Ignition phase of combustion process under low-gravity conditions.

[Color figure can be viewed in the online issue, which is available at www.interscience.wiley.com.]

a data acquisition board (Model PCI-MIO-16XE-50, National Instruments) supported by a software package (LabVIEW, National Instruments) are used to monitor the evolution of the synthesis reaction. During the synthesis process, samples were placed inside a steel vessel, where argon was maintained at a pressure equals to 2 *atm*. After reaction completion, the chamber was evacuated, refilled with argon and the sample holder replaced. A similar apparatus has been used to perform ground based experiments.[26]

The obtained products were characterized in terms of chemical composition and microstructure by X-ray diffraction (XRD) analysis (Philips PW-1830 diffractometer using Cu K_α Ni-filtered radiation), scanning electron microscopy (SEM), and electron dispersive spectroscopy (EDS) microanalysis (HITACHI S 4000 Field emission equipped with a KEVEX SIGMA 32 probe at a resolution of 142 eV).

Experimental Results and Discussion

In this work, the reduced gravity environment was obtained by a special airbus (Airbus A300) through series of parabolic maneuvers. Specifically, the aircraft starts from a steady normal horizontal flight, and then it takes a 1.8 *g* load factor nosing up to 45° and climbing to 9,000 m. Then the engine thrust is considerably reduced. When it overcomes the aerodynamic drag, the pilot kills the lift. This transition phase of *injection*, which separates the pull-up from the *zero g* parabola, lasts less than 5 s. The aircraft is then in the low-gravity phase for 25 *s*. A symmetrical pull-out phase is then executed on the down side of parabola to bring the aircraft to its steady horizontal flight in about 20 s. A normal mission lasts about 2 h, and consists of 30 parabolas. During each parabola gravity is lower than $2\ 10^{-2}\ g$.

Typically, ignition of the reaction was performed at the *injection* phase (the entry of zero *g* phase). Figure 4 shows an example of the ignition phase during parabolic flight experiments. It is worth noting that, when the configuration "cylindrical pellet + conical sample" was taken into account, the ignition phase was anticipated in order to guarantee the occurrence of reaction quenching under low-gravity conditions.

In Table 2, the reaction behavior of investigated systems is reported in terms of occurrence of self-propagating regime

Table 2. Reaction Behavior under Low-Gravity and Terrestrial Conditions

System	Self-propagation (10^{-2} g)	Self-propagation (1g)
TiB_2-$TiAl_3$	Yes	Yes
TiB_2-$2TiAl_3$	Yes	Yes
TiB_2-$3TiAl_3$	No	Yes
TiB_2-2TiAl	Yes	Yes
TiB_2-3TiAl	Yes	Yes
TiB_2-4TiAl	Yes	Yes

under both low-gravity and terrestrial conditions. While the TiB_2-$3TiAl_3$ system shows a self-propagating character under terrestrial conditions, the front reaction, once activated, is not able to advance spontaneously under low-*g* environment.

Figures 5 and 6 show the dependence of maximum temperature and front velocity, respectively, on the intermetallic/boride molar ratio (x). Experimental data obtained under terrestrial conditions are also reported for the sake of comparison. It was found that, regardless of gravity conditions, for both systems investigated, combustion temperature and propagating front velocity decrease when intermetallic/boride molar ratio is augmented. This behavior is related to the exothermicity of the reacting system, which decreases as the relative contribution of the most exothermic reaction involved, that is, the formation of TiB_2, is reduced. By comparing the results obtained under terrestrial and low-gravity environments, while maintaining system composition the same, maximum combustion temperature seems not significantly affected by gravity level. On the other hand, propagating front velocity resulted generally higher when reactions were performed under terrestrial conditions.

Analogous experimental evidences are reported in the literature on this field for other systems. In fact, experiments involving TiC-Al_2O_3-Al and ZrB_2-Al_2O_3-Al[8], Ni_3Al-TiB_2[10], NiAl-TiB_2[11,21], TiC-Al-Ni[13], HfB_2-Al, and HfB_2-Ni_3Ti[14] systems, all display relatively higher wave propagation velocities under terrestrial conditions, as compared to the corresponding values observed at low-gravity.

Regarding CFQ experiments Figure 7 shows, as an example, two quenched samples obtained for the case of TiB_2-$TiAl_3$ and TiB_2-$2TiAl_3$ systems, respectively. It is observed that combustion front is not flat once quenched. Moreover, a layer of unreacted powders close to the reacting mixture/copper block interface is found. This is likely due to the fact that the powders directly in contact with the copper block are maintained at relatively lower-temperatures, so that chemical transformations are not activated.

The traveled distance of the reaction front before extinction (measured starting from the base of the cone) is reported in Figure 8a and b, as a function of the intermetallic/boride molar ratio, for both low-gravity and 1*g* conditions. It is seen that the quenching distance decreases as the intermetallic/diboride molar ratio is augmented. These results are consistent since they both manifest the decrease of system reactivity when the intermetallic/boride molar ratio is increased. Moreover, extinction of combustion front is anticipated when the process is performed at low-gravity, as compared to the results obtained when the synthesis reaction takes place under terrestrial conditions. It should be noted that this experimental finding is in agreement with the relatively lower combustion front velocity observed under low-gravity conditions.

As an example of compositional characterization of the obtained products, XRD patterns of final products obtained during parabolic flights for the cases of the TiB_2-$2TiAl_3$ and TiB_2-2TiAl systems, are shown in Figure 9a and b, respectively. It is seen that the starting powders are completely converted to the desired phases for the case of the TiB_2-$2TiAl_3$ composite. Only in few cases the presence of small amounts of $Al_{11}Ti_5$ was also detected. However, when the TiB_2-2TiAl system was taken into account, Ti_3Al was also found in the composite along with the desired TiB_2 and TiAl phases. It is worth noting that the formation of significant amounts of Ti_3Al was also observed when preparing TiAl by field-activated combustion synthesis (FACS).[27]

Theoretical Analysis of Gravity Effects on Combustion Synthesis Processes

General considerations

On the basis of the experimental results shown in the previous section, as well as of the most significant ones reported

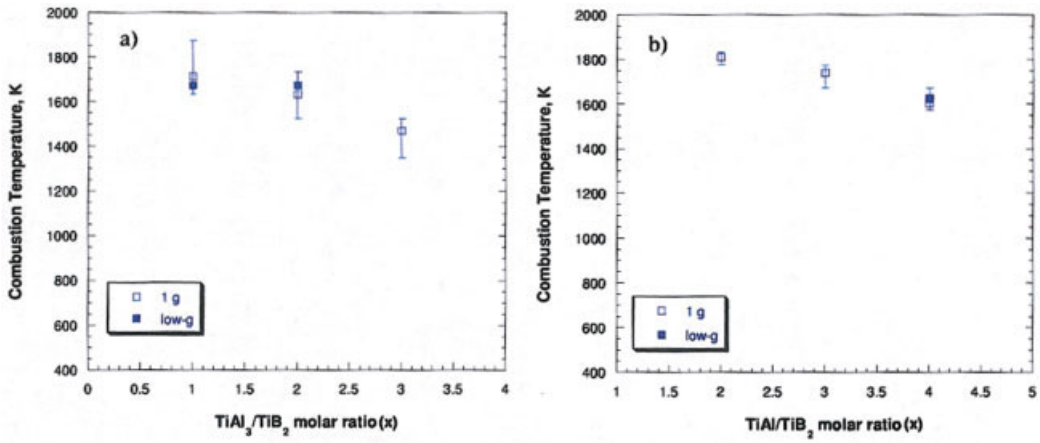

Figure 5. Comparison between maximum combustion temperature obtained under terrestrial and low-gravity conditions as a function of (a) TiB_2/$TiAl_3$, and (b) TiB_2/TiAl molar ratios.

[Color figure can be viewed in the online issue, which is available at www.interscience.wiley.com.]

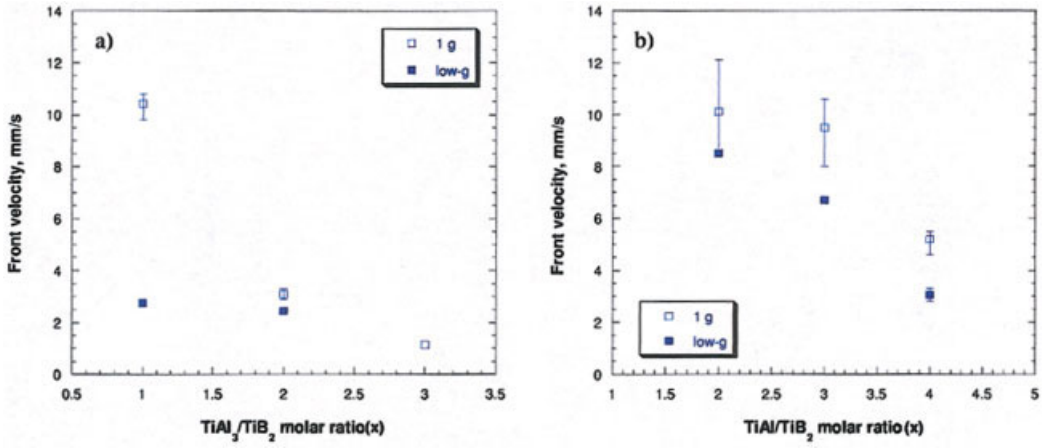

Figure 6. Comparison between front velocity obtained under terrestrial and low-gravity conditions as a function of (a) $TiB_2/TiAl_3$, and (b) $TiB_2/TiAl$ molar ratios.

[Color figure can be viewed in the online issue, which is available at www.interscience.wiley.com.]

in the literature on Combustion Synthesis performed under low-*g* conditions, some general conclusions can be drawn. Specifically, as compared to the corresponding behavior on the ground, combustion wave typically travels slower under reduced gravity. [8,10,11,13,14,21,24] Moreover, under terrestrial conditions, bottom ignition of the sample results in a higher-combustion velocity with respect to top ignition,[8,10,14,24] so that the following inequality holds: $U_{C_{low-g}} < U_{C_{1g}}^{top} < U_{C_{1g}}^{bottom}$. Besides, combustion temperature does not display a significant dependence on neither the gravitational level nor the ignition configuration.[8,24] Furthermore, final products synthesized in low-gravity environments, generally present finer and more uniform microstructure than those obtained under normal gravity conditions.[10,11,21,24]

Indeed, theoretical explanations of relatively lower combustion front velocity under reduced gravity conditions have not been provided yet in the literature, at least to our best knowledge. Justifications of negligible gravity effect on combustion temperature have also not been given. On the other hand, analysis regarding the effect of gravity on product microstructure are reported in the literature.[9,10,14,21,24] However, in our opinion, when dimensional analysis is performed for describing heat and mass-transfer phenomena involved in the combustion process, the choice of the characteristic length is not appropriate.

Figure 7. Direct comparison between TiB_2-$TiAl_3$ and TiB_2-$2TiAl_3$ final samples in the cylindrical and conical pellets configurations under low-gravity conditions.

[Color figure can be viewed in the online issue, which is available at www.interscience.wiley.com.]

In this work, a general, theoretical and thorough analysis of possible gravity effects on combustion synthesis is performed with the aim of explaining the experimental results summarized earlier. In particular, the influence of gravity on heat and mass transport taking place in the reacting sample at different length scales is examined along the lines represented in Figure 10. The arrows indicate the possible routes through which gravity may influence transport phenomena involved during combustion synthesis processes that, in turn, are responsible for the observed experimental findings. Specifically, gravity contribution to heat transfer within the so-called reaction zone (where most of the physicochemical phenomena typical of SHS take place[5]) is first analyzed. Next, gravity effect on product formation rate, which depends on heat and mass transport phenomena taking place at the microscopic level (that is, reactant particles and/or product grains), is investigated. This analysis along with the one related to *g*-level influence on heat losses from the pellet external surface, whose characteristic length can be identified with the pellet size (macroscopic level), allow to explain the experimental behavior of combustion temperature. Experimental results about combustion front velocity are then analyzed by considering the gravity effect on heat transfer within the reaction zone, combustion temperature, and product formation rate. Gravity influence on heat and mass transfer occurring at the microscopic scale is also taken into account in order to explain changes in product grain size obtained under different *g*-level environments. Finally, the role played by the gravitational field on product microstructure formation in terms of phase distribution is clarified by describing mass-transport phenomena at both macro and microscopic scale, and its effect on phase segregation.

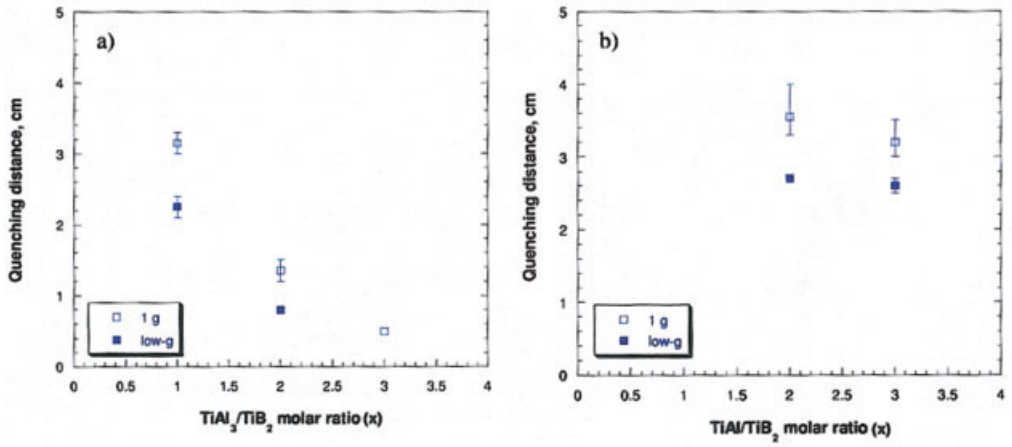

Figure 8. Comparison between quenching distances obtained under terrestrial and low-gravity conditions as a function of (a) $TiB_2/TiAl_3$, and (b) $TiB_2/TiAl$ molar ratios.

[Color figure can be viewed in the online issue, which is available at www.interscience.wiley.com.]

Effect of gravity on heat-transfer phenomena in the reaction zone

Several heat-transfer phenomena may contribute to heat transfer in the reaction zone which travels along the sample along with the propagation of the combustion wave. However, some of them, such as conduction within each solid, liquid or gaseous phase (the latter either present as inert gas or released during reaction), radiation between solid particles, capillary spreading of liquid phase inside the pores of the reacting pellet, as well as Marangoni flows due to surface tension gradients occurring at gas-liquid interfaces, are not affected by gravity. Therefore, they are not responsible for the different experimental results obtained under terrestrial and low-gravity environments. Conversely, as illustrated in what follows, other phenomena are gravity dependent and may contribute to affect heat transfer as g increases.

For sake of clarity, the different regions potentially present in the pellet during combustion synthesis processes are schematically reported in Figure 11. In particular, the reaction zone is further represented in terms of constituent phases and gravity-induced heat transport phenomena taking place. Obviously, since Figure 11 shows the most general situation, some of the regions reported may be not present, depending on the specific system under investigation.

Inside the two regions which consist of solid and gas phases only, unstable situations accompanied by natural convection of the gas phase inside the solid matrix (reactants or final products), may occur when temperature gradients are established.

The co-existence of solid, liquid and gaseous phases characterizes regions where solid reactants dissolve in molten reactants or diluents, as well as regions behind the combustion front where solid products crystallize from the molten phase. Typically, systems investigated under reduced gravity contain a large volume fraction of low-melting components (reactants, diluents or products). Therefore, regions where a liquid phase is present may be depicted as a continuous liquid phase with settling/buoyancing solid particles and gaseous bubbles. Within these regions, heat transfer driven by gravity-dependent phenomena, such as natural convection in liquid phase and Stokes motion of particles and bubbles, may take place.

Finally, a region consisting of a molten phase where no solids and buoyancing gaseous bubbles are present, respectively, may appear in reacting systems involving low-melting products. In these regions, natural convection phenomena and bubble motion may contribute to the overall heat transfer.

Furthermore, molten phase permeation induced by capillarity and gravity may occur inside solid matrices, which are in contact with regions where a liquid phase is present. In particular, depending on the relative direction of the wave propagation with respect to the g vector, gravity favors molten phase permeation into the solid products matrix, for the case of ignition from the pellet bottom side, while molten phase infiltration into the solid reactants matrix is favored when the pellet is ignited from the top-side. In this latter case, heat transfer in the reaction zone may increase as a consequence of the gravity favored liquid-phase transport.

It is now required to establish which, among the aforementioned heat-transfer phenomena, gives a significant contribution when compared to gravity independent heat transport mechanism.

Natural convection in the gas phase present within the solid matrix

Let us first focus on the regions consisting of a solid porous matrix (cf. Figure 11). As mentioned by Yi et al.[14], during combustion synthesis reactions, gaseous free convective flows driven by temperature gradients may take place when the ignition is performed on the sample bottom-side. In this case, combustion wave propagates in the opposite direction of gravity vector, and the unreacted pellet can be preheated by hot gases moving upward. Thus, since preheating of unreacted sample increases front velocity, it is worthwhile evaluating the relative importance of heat transfer by gas-phase natural convection, as compared to conduction. This comparison can be made by estimating the Rayleigh number which, for porous media, is expressed as follows[28]

$$Ra = \frac{\rho^2_{(gas)} C_{p,(gas)} \beta_{(gas)} g \Delta T K L^*}{\mu_{(gas)} k_x} \tag{3}$$

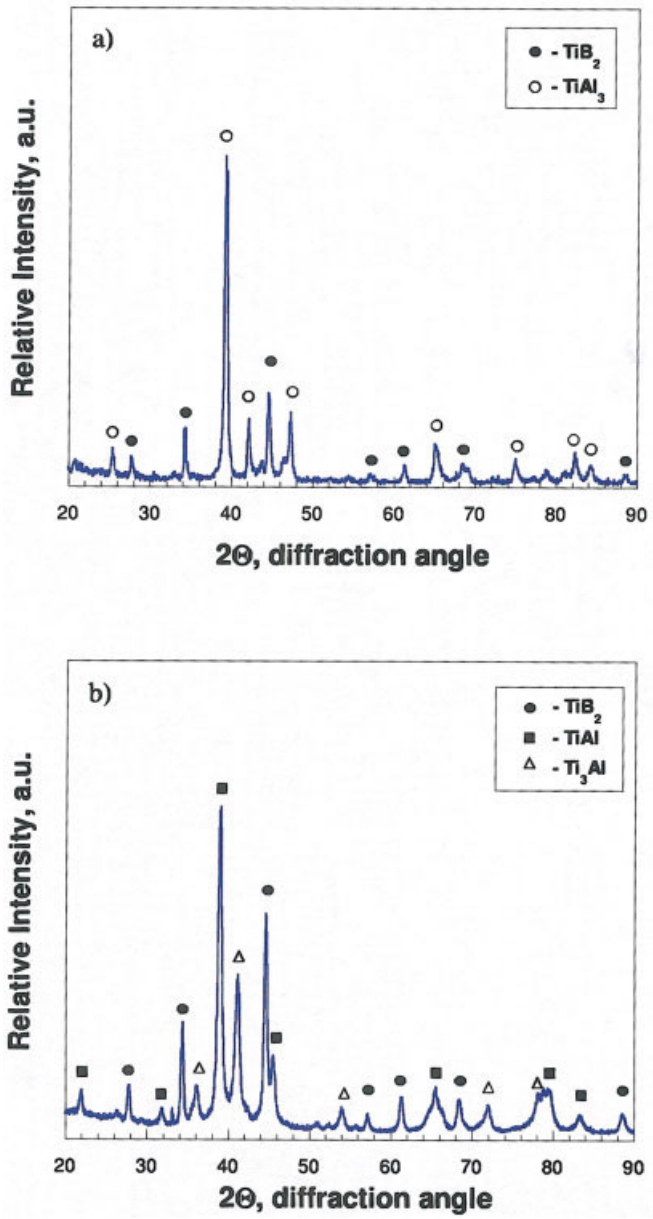

Figure 9. XRD diffraction pattern of final product obtained under low-gravity conditions for the case of the (a) TiB_2-2$TiAl_3$, and (b) TiB_2-2TiAl system.

[Color figure can be viewed in the online issue, which is available at www.interscience.wiley.com.]

Note that, above the critical Rayleigh number, that is, $Ra^* = 40$,[28] natural convection represents the dominant phenomenon. Porous reacting pellet permeability (K) can be determined by means of the Carman-Kozeny relationship[28]

$$K = \frac{d_p^2}{180}\frac{\varepsilon^3}{(1-\varepsilon)^2} \tag{4}$$

From Eqs. 3 and 4, it is seen that the relative importance of natural convection increases as the permeability increases (that is, as the porosity and the average particle size characterizing the reacting system increase).

An example of calculation of Rayleigh number is performed for a specific system whose properties are reported in Table 3. Specifically, it refers to a solid matrix with high-porosity consisting of coarse powders of titanium, widely used as starting reactant in combustion synthesis. From Eq. 4, the permeability of this system results to be equal to about $5.3\ 10^{-11}\ m^2$. The thermal conductivity (k_x) of the solid matrix is evaluated by the following relationship[32]

$$k_x = k_{(c)}\frac{1 + 2\lambda\phi + (2\lambda^3 - 0.1\lambda)\phi^2 + \phi^3 0.05\exp(4.5\lambda)}{(1-\lambda\phi)},$$

$$\lambda = \frac{k_{(d)} - k_{(c)}}{k_{(d)} + 2k_{(c)}} \tag{5}$$

where ϕ is the volume fraction of the dispersed phase, and $k_{(c)}$ and $k_{(d)}$ are the thermal conductivities of the continuous and dispersed phase, respectively. In order to be conservative, the gas has been assumed as the continuous phase while the solid particles represent the dispersed phase in Eq. 5.[32] Under these conditions, thermal conductivity of the porous matrix is about $0.16\ W\ m^{-1}\ K^{-1}$.

By substituting the obtained values in Eq.3, along with the thermophysical properties of argon also reported in Table 3, the resulting Rayleigh number is about $1.3\ 10^{-4}$, which is much smaller than Ra^*. Therefore, even under the adopted conservative conditions (that is, characteristic length of the same order of magnitude of pellet dimensions, high-temperature gradient, high porosity, coarse powders), *the contribution of natural convection within the gas phase to heat transfer in the reaction zone is negligible*. This result is mainly due to the relatively low-value of permeability characterizing packed samples made of micrometric powders. It should be noted that this theoretical outcome does not validate Yi et al.[14] conclusion that convective flow of argon gas was the major cause for the enhanced combustion front velocity for bottom ignition.

Molten-phase permeation within the solid matrix

Once a molten phase is formed, it may permeate through a solid matrix under the action of capillary and gravitational forces. If the pellet is ignited at its top-side, the gravity-enhanced liquid phase infiltration may preheat the reactants by increasing the heat transfer downward (cf. Figure 11). The relative importance of gravity with respect to capillarity can be evaluated by the specific Bond number (Bo) for porous media[33]

$$Bo = \frac{\rho_{(liq)} g K}{\gamma_{lv}} \tag{6}$$

The parameter values used for estimating Bo are reported in Table 4. In order to maximize the potential effect of gravity with respect to capillary forces, the value of permeability calculated in the previous paragraph and related to a highly porous solid matrix consisting of coarse powders, is used (conservative conditions). For the same reason, liquid hafnium at its melting temperature is chosen as the molten phase due to its high-density. Nevertheless, the resulting value of Bo is

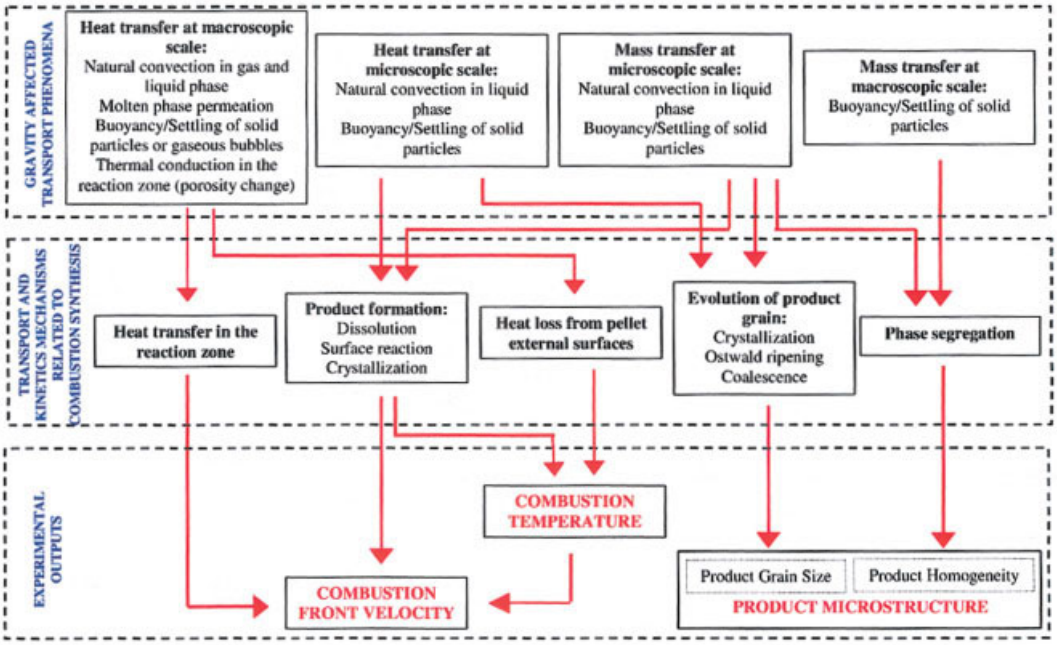

Figure 10. Representation of theoretical analysis performed.

[Color figure can be viewed in the online issue, which is available at www.interscience.wiley.com.]

about 3.8 10^{-6}, and, consequently, it can be concluded that *gravity does not affect permeation of molten phase during combustion synthesis processes*.

Solid particles or gas bubbles Stokes motion within the molten layer

A reliable estimate of the relative contribution of solid particle or gas-bubble motion to the overall heat transport in sample regions where a molten phase is present, can be obtained through the heat Peclet number Pe_H

$$Pe_H = \frac{(\rho C_p v_t)_{(particle\ or\ bubble)} L^*}{k_{(liq)}} \tag{7}$$

which represents the ratio between heat transfer due to particle or bubble motion, and that due to thermal conduction in the liquid phase. In particular, the height of the molten layer is assumed as characteristic length L^*. The particles/bubbles terminal velocity (v_t) is calculated by means of the Stokes' equation[35]

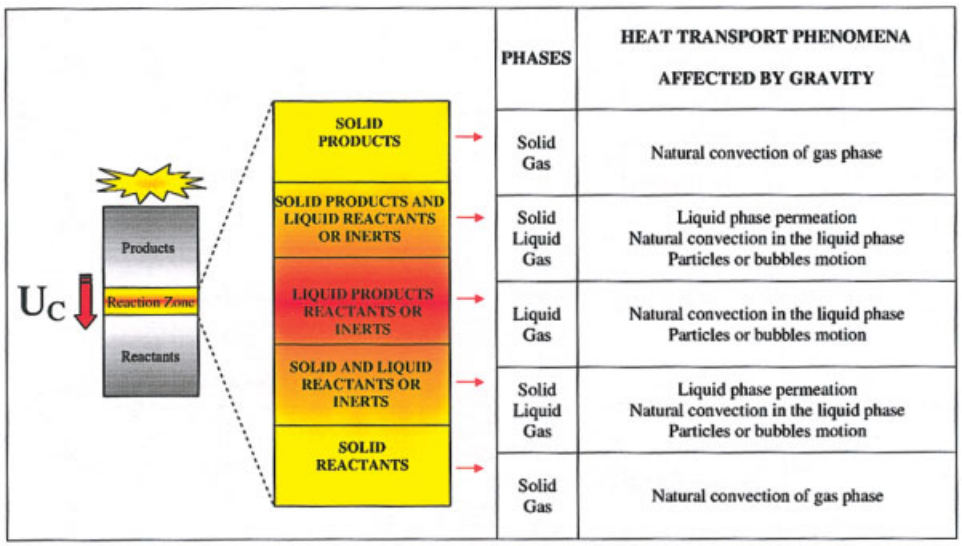

Figure 11. Representation of SHS process, as well as of the so-called reaction zone, in terms of constituent phases and of gravity-induced heat-transport phenomena taking place.

[Color figure can be viewed in the online issue, which is available at www.interscience.wiley.com.]

Table 3. Parameters to Evaluate the *Ra* Number in Eq. 3, that is, to Quantify Natural Convection in the Gas Phase within the Solid Matrix

Parameters	Units	Value	Reference
$\phi = (1 - \varepsilon)$	—	0.3	this work
d_p	μm	50	this work
T_C	K	3000	this work
$k_{(c)} = k_{(gas),\,Ar}$	$W\,m^{-1}\,K^{-1}$	$5.96\ 10^{-2}$	[29]
$k_{(d)} = k_{(s),\,Ti}$	$W\,m^{-1}\,K^{-1}$	25.8	[30]
L^*	m	0.01	this work
$C_{p,\,(gas),\,Ar}$	$J\,kg^{-1}\,K^{-1}$	520.3	[31]
$\rho_{(gas),\,Ar}(*)$	$kg\,m^{-3}$	0.583	[29]
$\beta_{(gas),\,Ar}$	K^{-1}	$6.06\ 10^{-4}$	[29]
$\mu_{(gas),\,Ar}$	$Pa\,s$	$7.49\ 10^{-5}$	[29]

Thermophysical properties of elements are evaluated at $T = (T_C + T_0)/2$ where $T_0 = 298\ K$.
(*)$P = 0.2\ MPa$.

$$\nu_t = \frac{d^2_{(particle/bubble)} g \left|\rho_{(particle/bubble)} - \rho_{(liq)}\right|}{18\,\mu_{(liq)}}; \qquad \left[\mathrm{Re}_p = \frac{\rho_{(liq)}(\nu_t d)_{(particle/bubble)}}{\mu_{(liq)}} < 0.1\right] \quad (8)$$

where d represents particles or bubbles average diameter.

Conservative conditions are adopted also in this case for enhancing Stokes motion and, thus, its contribution to heat transfer. In particular, coarse hafnium solid particles settling in liquid aluminum and large argon bubbles buoyancing in liquid hafnium, are considered when evaluating v_t and Pe_H (cf. Table 5). Hf solid particle terminal velocity results to be about 0.19 $m\ s^{-1}$, while bubbles move inside liquid Hf with a velocity equal to about $1.2\ 10^{-2}\ m\ s^{-1}$. Correspondingly, Eq. 7 provides $Pe_H = 32.5$, for settling hafnium solid particles in liquid aluminum, and $Pe_H = 6.4\ 10^{-4}$, for buoyancing argon bubbles in liquid hafnium.

These results clearly demonstrate that, *at least in principle, solid-particle sedimentation can contribute to the overall heat transfer, while gas bubble motion role may be reasonably neglected*. However, Stokes' law, that is, Eq. 8, deals with the motion of particles which do not interact with each other. Actually, when solid particles are present in the molten phase, the latter behaves like a suspension, whose apparent viscosity and density increase as particle concentration increases. This condition is often referred in the literature to hindered settling.[39] Thus, the value of v_t calculated above overestimates the real-particle velocity. However, these results show that by adopting very favorable (conservative) conditions, the contribution of solid particle settling to the overall heat transfer cannot be neglected. Therefore, it needs to be evaluated referring to the specific system under investigation.

As an example, the calculation earlier is performed for one of the systems experimentally studied during the parabolic flight campaign, (that is, TiB_2-$TiAl_3$). By using the data reported in Table 6, the terminal velocity of a spherical solid particle (TiB_2) in a molten phase (Ti-3Al) is about $7.9\ 10^{-2}\ \mu m\ s^{-1}$, while Pe_H results equal to about $4.4\ 10^{-5}$. It is worth noting that, due to the lack of experimental data for thermophysical properties of liquid metals alloys, ideal solution of elemental Ti and Al have been assumed, and, hence, the following mixing rules have been used

$$\Psi_{(j)} = \sum_i Z_{i,(j)}; \quad \left[\Psi = \frac{1}{\rho},\ Cp,\ k,\ \mu,\ \beta\right]; \qquad \left[Z_{i,(j)} = \frac{\omega_{i,(j)}}{\rho_i},\ \omega_{i,(j)} C_{pi},\ \phi_{i,(j)} k_i,\ \chi_{i,(j)}\mu_i,\ \chi_{i,(j)}\beta_i\right] \quad (9)$$

where i stands for the elemental constituents of the phase j (for example, the intermetallic liquid mixture). The very small Pe_H value obtained in this case leads to the conclusion that during combustion synthesis of TiB_2-$TiAl_3$, *heat transfer due to solid particle settling can be neglected in comparison to thermal conduction in the liquid phase*. An analogous result is obtained

Table 4. Parameters to Evaluate the *Bo* Number in Eq. 6, that is, to Quantify Molten Phase Permeation within the Solid Matrix

Parameter	Units	Value	Reference
K	m^2	$5.29\ 10^{-11}$	this work
$\rho_{(liq),\,Hf}$	$kg\,m^{-3}$	11820	[34]
$\gamma_{lv,\,Hf}$	$J\,m^{-2}$	1.62	[34]

Thermophysical properties of liquid Hafnium are evaluated at $T = 2{,}500\ K$.

Table 5. Parameters to Evaluate the Pe_H Number in Eq. 7, that is, to Quantify Solid Particles or Gas Bubbles Stokes Motion within the Molten Layer

Parameter	Units	Value	Reference
$d_{(particle/bubble)}$	μm	100	this work
$\rho_{(s),\,Hf}$	$kg\,m^{-3}$	13280	[30]
$\rho_{(liq),\,Hf}$	$kg\,m^{-3}$	11820	[34]
$\rho_{(liq),\,Al}$	$kg\,m^{-3}$	1890	[36]
$\rho_{(gas),\,Ar}(*)$	$kg\,m^{-3}$	0.389	[29]
$\mu_{(liq),\,Hf}$	$Pa\,s$	$5.20\ 10^{-3}$	[34]
$\mu_{(liq),\,Al}$	$Pa\,s$	$3.23\ 10^{-4}$	[37]
L^*	m	0.01	this work
$C_{p,(gas),\,Ar}$	$J\,kg^{-1}\,K^{-1}$	520.3	[31]
$C_{p,(s),\,Hf}$	$J\,kg^{-1}\,K^{-1}$	206.3	[31]
$k_{(liq),\,Al}$	$J\,kg^{-1}\,K^{-1}$	144.3	[38]
$k_{(liq),\,Hf}$	$J\,kg^{-1}\,K^{-1}$	39.0	[38]

Thermophysical properties of elements are evaluated at $T = 2500\ K$.
(*)$P = 0.2\ MPa$.

Table 6. Parameters to Evaluate the Pe_H Number in Eq. 7 for the Case of the Combustion Synthesis of TiB_2-$TiAl_3$ Composites, that is, to Quantify Stokes Motion of Solid Particles within the Molten Layer

Parameter	Units	Value	Reference
$d_{p,\,TiB_2}$	μm	0.2	this work
ρ_{TiB_2}	$kg\,m^{-3}$	4520	[30]
$C_{p,\,TiB_2}$	$J\,kg^{-1}\,K^{-1}$	1403	[31]
$\rho_{(liq),\,Al}$	$kg\,m^{-3}$	1961	[36]
$\rho_{(liq),\,Ti}$	$kg\,m^{-3}$	4041	[40]
$\rho_{(liq)}$	$kg\,m^{-3}$	2424	Eq. 9
$\mu_{(liq),\,Al}$	$Pa\,s$	$3.57\ 10^{-4}$	[37]
$\mu_{(liq),\,Ti}$	$Pa\,s$	$1.24\ 10^{-3}$	[37]
$\mu_{(liq)}$	$Pa\,s$	$5.78\ 10^{-4}$	Eq. 9
L^*	m	0.01	this work
$k_{(liq),\,Al}$	$W\,m^{-1}\,K^{-1}$	136.6	[38]
$k_{(liq),\,Ti}$	$W\,m^{-1}\,K^{-1}$	35.1	[41]
$k_{(liq)}$	$W\,m^{-1}\,K^{-1}$	113.9	Eq. 9

Thermophysical properties of elements are evaluated at $T = 2273\ K$.

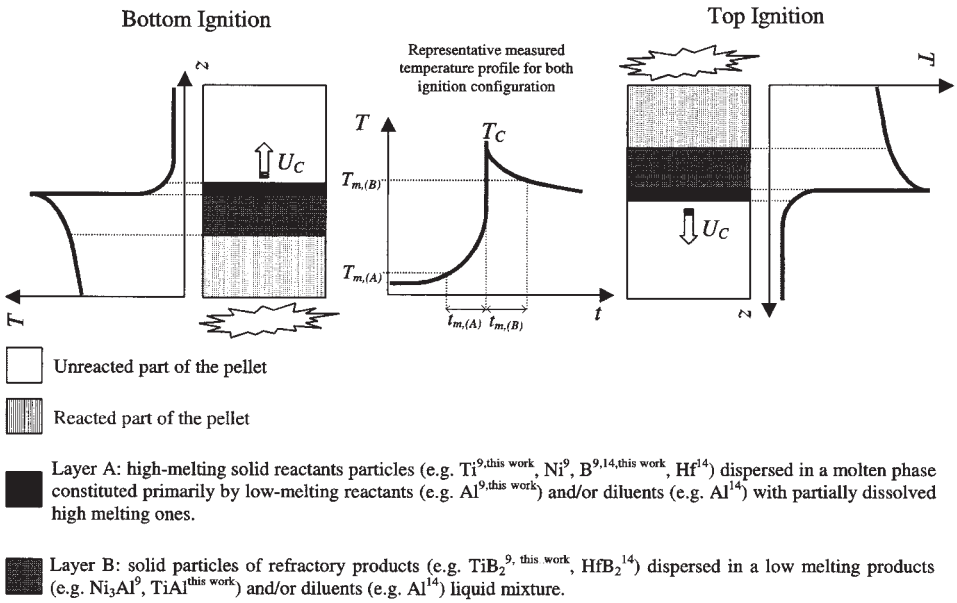

Figure 12. Ignition configurations of SHS process and related temperature profiles.

for the other titanium diboride-titanium aluminide composites investigated during the parabolic flight campaign.

It is apparent that, the opposite conclusion drawn in this case as compared to that resulting when using the data reported in Table 5, mainly depends on the large differences in particle size used in the two examples.

Natural convection within the molten layer

In order to evaluate if natural convection in the liquid phase plays a significant role under terrestrial gravity, the following condition

$$Ra = \frac{\rho^2_{(liq)} C_{p,(liq)} \beta_{(liq)} g \Delta T L^{*3}}{\mu_{(liq)} k_{(liq)}} > Ra^* \qquad (10)$$

needs to be verified.[42] In this expression, ΔT is the temperature difference within the melt, and L^* is the characteristic length (that is, height of the melt) over which ΔT is established. The Rayleigh critical value (Ra^*) for the case of an infinite horizontal layer falls in the range 657 – 1708, depending on the type of boundary conditions applied during its derivation.[42]

In Figure 12 additional details of the combustion synthesis process with respect of the ones given in Figure 11 are reported. In particular, wave propagation directions, representative temperature profiles, and reaction zone are shown for the top and bottom ignition configurations.[1-5,24] It may be seen that two different layers containing a liquid phase may appear in the reaction zone. The layer, hereafter, indicated with A is the one adjacent to the unreacted part of the pellet. It is characterized by the presence of high-melting solid reactants particles dispersed in a molten phase, constituted primarily by low-melting reactants and/or diluents with partially dissolved high-melting ones. Instead, solid particles of refractory products dispersed in a low-melting products and/or diluents liquid mixture form the layer (labeled as B) adjacent to the reacted part of the sample.

Consequently, natural convection in combustion synthesis takes place in layer A or B reported in Figure 12, depending on the orientation of the front propagation with respect to gravity vector. Specifically, for the case of ignition from the bottom-side of the sample, natural convection takes place in the layer A, while in the opposite configuration (ignition from the sample top side), natural convection occurs in the layer B.

In the sequel, the calculation of *Ra* is performed for one of the systems (that is, TiB_2/Ni_3Al) for which the effect of ignition configuration on combustion behavior has been experimentally studied.[9] In particular, Rayleigh number is calculated by using the thermophysical parameters reported in Table 7, and referred to molten aluminum, and a 3Ni-Al liquid mixture for layer A (bottom ignition) and B (top ignition), respectively. The height of the molten layers (L^*) are estimated by multiplying the experimentally measured combustion front velocity (U_C), with the time during which the liquid phases exists, $t_{m,(A)}$ and $t_{m,(B)}$, evaluated as shown in the representative temperature temporal profile reported in Figure 12. The latter are obtained from the unique experimental profile reported by the authors. Based on data reported in Table 7 $Ra = 6.25\ 10^4$ and $Ra = 1.47\ 10^6$ for layer A and B are obtained, respectively.

Therefore, it can be concluded that since condition (10) is verified for both ignition configuration, *free convection phenomena in the liquid phase are likely to play a role during combustion synthesis of the nickel aluminides-titanium diborides composites*. Similar conclusions can be drawn when considering the system HfB_2/Al,[14] as well as the system TiB_2/2TiAl investigated in this work only under the top ignition configuration.

Effect of gravity on product formation rate

Conversion of initial solid reactants to final solid products during Combustion Synthesis processes involves several phenomena, such as dissolution of solid reactant particles into a liquid phase, surface reaction between solid and molten reactants, product crystallization from liquid solutions. The latter

Table 7. Parameters to Evaluate the *Ra* Number in Eq. 10 for the Case of the Combustion Synthesis of TiB_2-3NiAl Composites, that is, to Quantify Natural Convection within the Molten Phase

Parameter	Units	Value	Reference
Layer A for the case of bottom ignition[(1)]			
$\beta_{(liq),\,Al}$	K^{-1}	$1.43\ 10^{-4}$	[36]
$\rho_{(liq),\,Al}$	$kg\ m^{-3}$	2179	[36]
$\mu_{(liq),\,Al}$	$Pa\ s$	$5.28\ 10^{-4}$	[37]
$k_{(liq),\,Al}$	$W\ m^{-1}\ K^{-1}$	112.6	[38]
$C_{p,(liq),\,Al}$	$J\ kg^{-1}\ K^{-1}$	1177	[31]
$T_{m,\,Al}$	K	933	[31]
$\Delta T = T_C - T_{m,\,Al}$	K	1273[(2)]	this work
U_C	$m\ s^{-1}$	$3.6\ 10^{-2}$	[9]
$t_{m,(A)}$	s	0.2	[9]
L^*	m	$7.2\ 10^{-3}$	[9]
Layer B for the case of top ignition[(3)]			
$\beta_{(liq),\,Al}$	K^{-1}	$1.51\ 10^{-4}$	[46]
$\beta_{(liq),\,Ni}$	K^{-1}	$8.23\ 10^{-5}$	[43]
$\beta_{(liq),\,mix}$	K^{-1}	$9.22\ 10^{-5}$	Eq. 9
$\rho_{(liq),\,Al}$	$kg\ m^{-3}$	2065	[36]
$\rho_{(liq),\,Ni}$	$kg\ m^{-3}$	7728	[43]
$\rho_{(liq),\,mix}$	$kg\ m^{-3}$	5722	Eq. 9
$\mu_{(liq),\,Al}$	$Pa\ s$	$4.15\ 10^{-4}$	[37]
$\mu_{(liq),\,Ni}$	$Pa\ s$	$3.74\ 10^{-3}$	[37]
$\mu_{(liq),\,mix}$	$Pa\ s$	$2.91\ 10^{-3}$	Eq. 9
$k_{(liq),\,Al}$	$W\ m^{-1}\ K^{-1}$	125.1	[38]
$k_{(liq),\,Ni}$	$W\ m^{-1}\ K^{-1}$	60.0	[38]
$k_{(liq),\,mix}$	$W\ m^{-1}\ K^{-1}$	83.3	Eq. 9
$C_{p,(liq),\,Al}$	$J\ kg^{-1}\ K^{-1}$	1177	[31]
$C_{p,(liq),\,Ni}$	$J\ kg^{-1}\ K^{-1}$	734.2	[31]
$C_{p,(liq),\,mix}$	$J\ kg^{-1}\ K^{-1}$	793.0	Eq. 9
T_{m,Ni_3Al}	K	1668	[9]
$\Delta T = T_C - T_{m,Ni_3Al}$	K	538[(2)]	this work
U_C	$m\ s^{-1}$	$3.2\ 10^{-2}$	[9]
$t_{m,(B)}$	s	9.1	[9]
L^*	m	$3\ 10^{-2}$ [(4)]	[9]

[(1)]Thermophysical properties of liquid Al have been evaluated at $T = (T_C + T_{m,Al})/2$.
[(2)]$T_C = 2206\ K$[9].
[(3)]Thermophysical properties of liquid Al and Ni have been evaluated at $T = (T_C + T_{m,Ni_3Al})/2$.
[(4)]*Since* $U_C \cdot t_{m,(B)} > L$, the pellet length has been assumed as characteristic length.

phenomenon takes place either through nucleation and grain growth under supersaturation or solidification driven by undercooling conditions. The rate at which all the aforementioned phenomena occur determines the overall product formation rate. It depends on temperature and concentrations distributions around dissolving, reacting, crystallizing or solidifying particles/grains. Therefore, in order to evaluate the gravity influence on the rate of product formation kinetics, a thorough analysis of the effect of gravity on heat and mass transfer at the particle scale is carried out.

Gravity can induce natural convection due to thermal and concentration gradients in the liquid phase surrounding solid particles. Moreover, in presence of gravitational loads, solid particles move also by settling/buoyancy within the liquid phase. A way to estimate the effects of these gravity-induced phenomena on heat and mass transfer takes advantage of the dimensional analysis. In particular, for a spherical particle in a liquid, heat and mass-transfer coefficients are given, respectively, by the following general correlations[44]

$$Nu = 2 + \varphi(\mathrm{Re}_p, \mathrm{Pr}) + \psi(Gr_H, \mathrm{Pr}) \tag{11}$$

$$Sh = 2 + \varphi(\mathrm{Re}_p, Sc) + \psi(Gr_M, Sc) \tag{12}$$

where the dimensionless numbers are expressed as follows

$$Nu = \frac{h d_p}{k_{(liq)}} \tag{13}$$

$$Sh = \frac{k_m d_p}{D_m} \tag{14}$$

$$\mathrm{Re}_p = \frac{\rho_{(liq)} \nu_t d_p}{\mu_{(liq)}} \tag{15}$$

$$\mathrm{Pr} = \frac{C_{p,(liq)} \mu_{(liq)}}{k_{(liq)}} \tag{16}$$

$$Sc = \frac{\mu_{(liq)}}{\rho_{(liq)} D_m} \tag{17}$$

$$Gr_H = \frac{\rho^2_{(liq)} \beta_{(liq)} g \Delta T d_p^3}{\mu^2_{(liq)}} \tag{18}$$

$$Gr_M = \frac{\rho_{(liq)} g \Delta \rho_{(liq)} d_p^3}{\mu^2_{(liq)}} \tag{19}$$

The first terms on the righthand side of both Eqs. 11 and 12 represent the contribution to heat and mass transfer by pure molecular conduction and diffusion, respectively. The second terms are responsible for heat and mass transfer due to solid particle motion as a consequence of settling/buoyancy phenomena. Natural convection in the liquid phase induced by temperature and concentration gradients is taken into account by the third terms in Eqs. 11 and 12. In all the dimensionless groups considered, the characteristic length is the diameter (d_p) of the particle undergoing dissolution, surface reaction, or crystallization.

Actually, when surface tension gradients existing at the gas-liquid interface (Marangoni flow) contribute significantly to heat and mass transfer, two additional terms, that is, $\xi(Ma_H,Pr)$ (see for example, refer [45]), and $\xi(Ma_M,Sc)$,[46] need to be added to Eqs. 11 and 12, respectively. However, it is well known that Marangoni flow, as well as molecular conduction and diffusion are not gravity-dependent. Thus, it is straightforward that gravity is expected to play a significant role during product formation (reaction), only if Nusselt and Sherwood numbers under terrestrial conditions are significantly greater than $2+\xi(Ma_H,Pr)$ and $2+\xi(Ma_M,Sc)$, respectively.

While the increase of Marangoni flow to heat and mass transfer do not need to be evaluated, contributions to heat and mass-transport coefficients by solid-particle motion (φ), and natural convection in the liquid phase (ψ) can be estimated through the following correlations[35,44,47]

$$\varphi(\mathrm{Re}_p, \mathrm{Pr}) = 0.47\ \mathrm{Re}_p^{1/2}\mathrm{Pr}^{0.363}; \quad [Re_p = 102 \div 5\ 10^4; Pr = 1\ 10^{-3} \div 101] \tag{20}$$

Table 8. Parameters to Evaluate *Nu* and *Sh* Numbers in Eqs. 11 and 12, that is, to Quantify Heat and Mass Transfer at the Microscopic Scale

Parameter [units]	Value(*)			Reference
T_m [K]		923–2750		[31]
$\rho_{(liq)l}$ [kg m^{-3}]		1588–11820		[34, 36, 37, 40, 43]
$C_{p,(liq)}$ [J kg^{-1} K^{-1}]		187.5–1343		[31]
$\mu_{(liq)}$ [mPa s]		0.80–5.70		[34, 37]
$k_{(liq)}$ [W m^{-1} K^{-1}]		30–163		[38, 41]
R_a [nm]		0.117–0.160		[30]
D_m [m^2 s^{-1}]		$1.87\ 10^{-9}$–$1.32\ 10^{-8}$		[48](**)
β [K^{-1}]		$4.35\ 10^{-5}$–$1.31\ 10^{-4}$		[10, 34, 36, 40, 43]
$\Delta\rho/\rho$		0.41–1.53		this work
Pr		0.0127–0.137		this work
Sc		24–664		this work
d_p [μm]	0.1	1	10	this work
v_t [$\mu m/s$]	$1.56\ 10^{-3}$–$7.33\ 10^{-2}$	0.156–7.33	15.6–733	this work
Re_p	$3.61\ 10^{-10}$–$2.30\ 10^{-8}$	$3.61\ 10^{-7}$–$2.30\ 10^{-5}$	$3.61\ 10^{-4}$–$2.30\ 10^{-2}$	this work
Gr_H	$1.06\ 10^{-9}$–$2.45\ 10^{-8}$	$1.06\ 10^{-6}$–$2.45\ 10^{-5}$	$1.06\ 10^{-3}$–$2.45\ 10^{-2}$	this work
Gr_M	$2.75\ 10^{-9}$–$1.02\ 10^{-6}$	$2.75\ 10^{-6}$–$1.02\ 10^{-3}$	$2.75\ 10^{-3}$–1.02	this work
$\varphi(Re_p,Pr)$	$2.17\ 10^{-6}$–$1.38\ 10^{-5}$	$6.88\ 10^{-5}$–$4.37\ 10^{-4}$	$2.18\ 10^{-3}$–$1.38\ 10^{-2}$	this work
$\psi(Gr_H,Pr)$	$1.02\ 10^{-3}$–$2.40\ 10^{-3}$	$5.76\ 10^{-3}$–$1.35\ 10^{-2}$	$3.24\ 10^{-2}$–$7.59\ 10^{-2}$	this work
$\varphi(Re_p,Sc)$	$2.50\ 10^{-6}$–$1.71\ 10^{-5}$	$1.81\ 10^{-4}$–$1.24\ 10^{-3}$	$1.31\ 10^{-2}$–$8.98\ 10^{-2}$	this work
$\psi(Gr_M,Sc)$	$1.64\ 10^{-2}$–$5.69\ 10^{-2}$	$9.25\ 10^{-2}$–$0.32\ 10^{-1}$	0.52–1.80	this work

(*) Thermophysical properties refer to the following liquid metals: Al, Cu, Cr, Co, Fe, Hf, Mg, Nb, Ni, Si, Ti, Zr.
(**)Self diffusion coefficients estimated through Stokes-Einstein equation.

$$\psi(Gr_H, \mathrm{Pr}) = 0.60 Gr_H^{1/4} \mathrm{Pr}^{1/3}; \quad [Gr^{1/4} Pr^{1/3} < 200] \tag{21}$$

$$\varphi(\mathrm{Re}_p, Sc) = 0.347 (Re_p Sc^{0.5})^{0.62}; \quad [Re_p Sc^{0.5} = 1.8 \div 6\ 10^5; \; Sc = 0.6 \div 3200] \tag{22}$$

$$\psi(Gr_M, Sc) = 0.569 (Gr_M Sc)^{0.25}; \quad [Gr_M Sc < 10^8] \tag{23}$$

along with the parameters reported in Table 8. In particular, thermophysical properties refer to liquid metals at the melting point, which are conditions typically attained during combustion synthesis processes. The range of particle diameter investigated is also characteristic of combustion synthesized products. In order to maximize the effect of gravity when evaluating Re_p, terminal velocity of solids settling in molten phase is calculated referring to particles of the relatively high-specific gravity compound HfB_2. Moreover, as a conservative condition, the temperature driving force appearing in Gr_H has been set equal to (3,500 − $T_m[K]$), where T_m is the metal melting temperature.

As can be seen in Table 8, contributions to the heat-transfer coefficient due to particle motion, and natural convection are in the ranges $2.17\ 10^{-6}$ −$1.38\ 10^{-2}$, and $1.33\ 10^{-3}$ − $8.88\ 10^{-2}$, respectively. In addition, the same Table shows that the terms related to the mass-transfer coefficient fall in the range $2.47\ 10^{-6}$ − $9.32\ 10^{-2}$, and $1.69\ 10^{-2}$ − 1.80, for particle motion and free convection, respectively. It should be noted that due to the limited availability of correlations for heat and mass transfer under low-Reynolds regime for the case of liquid metals, Eqs. 20 and 22 have been used even if the Re_p values obtained (cf. Table 8) do not fall within the prescribed range of the adopted relationships.

By analyzing the results reported in Table 8, it is seen that, as expected, gravity contribution to heat and mass transfer increases as solid particle diameter increases. However, only $\psi(Gr_M,Sc)$ becomes significant (same order of magnitude than molecular diffusion contribution) for large particles diameter ($\geq 10\ \mu m$).

From the analysis of the experimental results reported in the literature on Combustion Synthesis processes performed under low-g conditions, the maximum value of product grains is 3 μm.[9] Thus, it is possible to conclude that *heat and mass transfer-controlled phenomena involved in the product formation, such as dissolution, surface reaction, as well as crystallization are not influenced by gravity.*

Effect of gravity on combustion temperature

Combustion temperature depends on heat released by chemical transformations occurring during the process, as well as heat lost from external surfaces of the reacting pellet to the surroundings. The latter may be affected by gravity through natural convection within the gas phase present inside the reaction chamber. Specifically, in order to quantify the contribution of heat losses by natural convection from external surfaces with respect to radiation, the ratio between Biot and Stefan numbers has been considered

$$\frac{Bi}{St} = \frac{h}{\sigma T_C^3}. \tag{24}$$

By considering a cylindrical reacting pellet in vertical position, the heat transfer coefficient due to free convection is estimated by means of the following equation[49]

$$Nu^{1/2} = 0.68^{1/2} + \left(\frac{Gr_H \mathrm{Pr}/300}{[1 + (0.5/\mathrm{Pr})^{9/16}]^{16/9}} \right)^{1/6} \tag{25}$$

that fits experimental data over a wide range of Grashof and Prandtl numbers. Nusselt, Grashof and Prandtl numbers appearing in Eq. 25 are expressed as

Table 9. Parameters to Evaluate the Heat-Transfer Coefficient *h* in Eq. 26, that is, to Quantify Natural Convection in the Gas Phase Surrounding the Reacting Pellet

Parameter	Units	Value	Reference
L^*	m	0.02	this work
T_C	K	1773	this work
T_0	K	298	this work
P	MPa	0.2	this work
$C_{p,(gas),\,Ar}$	$J\ kg^{-1}\ K^{-1}$	520.3	[31]
$\rho_{(gas),\,Ar}$	$kg\ m^{-3}$	0.940	[29]
$k_{(gas),\,Ar}$	$W\ m^{-1}\ K^{-1}$	$4.29\ 10^{-2}$	[29]
$\beta_{(gas),\,Ar}$	K^{-1}	$9.66\ 10^{-4}$	[29]
$\mu_{(gas),\,Ar}$	$Pa\ s$	$5.53\ 10^{-5}$	[29]

Thermophysical properties of argon are evaluated at $(T_C + T_0)/2$.

$$Nu = \frac{hL^*}{k_{(gas)}} \tag{26}$$

$$Gr_H = \frac{\rho^2_{(gas)}\beta_{(gas)}g\Delta TL^{*3}}{\mu^2_{(gas)}} \tag{27}$$

and

$$\mathrm{Pr} = \frac{C_{p,(gas)}\mu_{(gas)}}{k_{(gas)}} \tag{28}$$

respectively, where the pellet length is assumed as characteristic length L^*. In order to estimate the value of h through Eq. 26, data reported in Table 9 are used, and a relatively low-combustion temperature is adopted for maximizing the effect of natural convection with respect to radiation (conservative conditions).

The obtained value of the heat-transfer coefficient is about $14\ W\ m^{-2}\ K^{-1}$, which allows one to evaluate by means of Eq. 24 the ratio *Bi/St* as equal to about 0.04. This result leads to the conclusion that because natural convection gives a negligible contribution, *gravity is not expected to affect the heat losses during combustion synthesis process.*

In addition, in the previous section it is shown that gravity has no significant effect on product formation, which determines the rate of heat generation. These findings clearly indicates that *gravity is not expected to affect* T_C, and provides a reasonable justification for the general experimental result (that is, negligible difference observed in combustion temperature when operating under terrestrial and reduced gravity conditions).

Effect of gravity on combustion-front velocity

Let us now try to clarify the reason why the combustion wave typically travels slower under low-gravity conditions. Several experimental and theoretical studies have demonstrated that enhanced heat transfer in the reaction zone, higher-combustion temperature, or reaction rate correspond to faster combustion wave propagation.[2,50,51] In particular, front velocity taking place during SHS reactions may be evaluated, under certain simplifying assumptions, through the following expression[5]

$$U_C = \sqrt{\frac{k_{mix}k_0}{\rho_0\Delta H_R}\left(\frac{RT_C^2}{E}\right)\exp\left(-\frac{E}{RT_C}\right)} \tag{29}$$

The latter one is specifically used for estimating activation energy E from experimental measurements of front velocity U_C, and combustion temperature T_C. According to this equation, U_C increases when at least one among T_C, the kinetic parameter (k_0), and the apparent thermal conductivity of the reacting medium (k_{mix}) increases. However, from the considerations reported in the previous section, gravity is not expected to affect T_C. Regarding this finding, it is worth noting that if the reduction of heat losses by natural convection would have been significant (that is, $Bi/St \geq 1$) when moving from terrestrial to low-g conditions, T_C should increase and combustion front should propagate faster, according to Eq. 29. This is just the opposite behavior of the experimental evidence. Therefore, *the responsibility of heat loss by natural convection for* U_C *decreasing when gravity level decreases can be excluded.*

Regarding the kinetic parameter k_0 appearing in Eq. 29, it should be mentioned that, in the framework of the assumptions made to obtain Eq. 29, that is, adiabatic conditions, infinite pellet length, first-order reaction with respect to the limiting reactant, Frank-Kamenetskii approximation, it represents a lumped parameter which accounts for several physicochemical mechanisms involved in product formation during SHS reactions, that is, dissolution of solid reactant particles into a liquid phase, surface reaction between solid and molten reactants, products crystallization from liquid solutions. However, since these heat and mass transfer-controlled phenomena are not influenced by gravity, it is also possible to state that *the kinetic parameter* k_0 *is expected to be insensitive to variations of the gravitational level.*

As for the apparent thermal conductivity of the reacting medium (k_{mix}), it may be regarded as a lumped parameter which accounts for all heat-transfer phenomena taking place inside the reaction zone, that is, thermal conduction, radiation, natural convection, and so on. In particular, k_{mix} should be higher under terrestrial than under low-gravity conditions, since some gravity-dependent heat-transport phenomena may increase it as g increases. Consequently, on the basis of Eq. 29, reaction front should propagate faster on the ground, as found experimentally.

In order to identify such phenomena, it should be noted that, as reported in the literature,[6,8,10,11,24] materials synthesized under low-g environments are typically characterized by higher porosity (sample elongation), with respect to those produced under terrestrial conditions. It is apparent, also from Eq. 5, that this leads to a variation of the thermal conductivity (k_x) of the reacting medium. To evaluate the magnitude of thermal conductivity change as porosity varies, let us consider the case of the system TiB_2/2TiAl, investigated in this work under the conditions reported in the experimental section. In particular, by assuming sample elongation in the range 0 – 4 mm, that is, pellet expansion of 0 – 20%, porosity increases from 0.45 to 0.55. Correspondingly, as shown in Table 10, the thermal conductivity (k_x) of the reaction zone invariably decreases regardless the specific phases present in this region. *Thus, as gravity is decreased from terrestrial conditions to low-gravity environment*, thermal conduction is depressed and, consequently, *the apparent thermal conductivity of the reacting*

Table 10. Effect of Pellet Expansion on Thermal Conductivity of the Reaction Zone

Description of Reaction Zone Structure	ρ [kg/m^3]	Ref.	k [W/m K]	Ref.	k_x [W/m K] $\Delta L = 0\%$	k_x [W/m K] $\Delta L = 10\%$	k_x [W/m K] $\Delta L = 20\%$
Porous matrix							
	$Ti_{(s)}$ 4510	[30]	$Ti_{(s)}$ 19.4	[30]			
(Only solid reactants with	$B_{(s)}$ 2470	[30]	$B_{(s)}$ 12.0	[39]	36.8(*)	31.8(*)	27.8(*)
pore filled by Ar)	$Al_{(s)}$ 2700	[30]	$Al_{(s)}$ 231.4	[39]			
Slurry							
(Molten Al with solid Ti	$Ti_{(s)}$ 4510	[30]	$Ti_{(s)}$ 20.4	[30]			
and B particles, and Ar	$B_{(s)}$ 2470	[30]	$B_{(s)}$ 11.8	[39]	24.9(**)	22.8(**)	20.9(**)
bubbles)	$Al_{(liq)}$ 2377	[36]	$Al_{(liq)}$ 91.0	[38]			
Molten layer							
	$Ti_{(liq)}$ 4281	[40]	$Ti_{(liq)}$ 28.0	[41]			
(Reactants liquid solution	$B_{(liq)}$ 2310	[52]	$B_{(liq)}$ 11.5	[39]	37.5(***)	34.1(***)	31.3(***)
with Ar bubbles)	$Al_{(liq)}$ 2108	[36]	$Al_{(liq)}$ 120.5	[38]			

(*) Eq. 5, where $k_{(c)} = k_{(s)} = \Sigma_i \phi_{i,(s)} k_{i,(s)}; i$ = Ti, Al, B and $k_{(d)} = k_{Ar,(gas)} = 2.98\ 10^{-2}$ *W/m K*.[29] Thermal conductivities are evaluated at $T = (T_{m,Al} + T_0)/2$ where $T_{m,Al} = 933.15$ *K* and $T_0 = 298.15$ *K*.

(**) Eq. 5, where $k_{(c)} = k_{(f)} = \phi_{Al,(f)} k_{Al,(liq)} + \phi_{Ar,(f)} k_{Ar,(gas)}$, ($k_{Ar,(gas)} = 3.99\ 10^{-2}$ *W/m K*[29]), and $k_{(d)} = k_{(s)} = \Sigma_i \phi_{i,(s)} k_{i,(s)}; i$ = Ti, B. Thermal conductivities are evaluated at $T = T_{m,Al} = 933.15$ *K*.

(***) $k_x = k_{(f)} = \Sigma_i (\phi_{i,(f)} k_{i,(liq)}) + \phi_{Ar,(f)} k_{Ar,(gas)}; i$ = Ti, B, Al, $k_{Ar,(gas)} = 6.41\ 10^{-2}$ W/m K.[29] Thermal conductivities are evaluated at $T_C = 1800$ *K* (cf. Figure 5b).

Note that volumetric fractions have been calculated on the basis of experimental conditions (stoichiometry, pellet dimensions, initial green density) reported in the experimental section.

medium (k_{mix}) is expected to be reduced. Accordingly, experimental evidences on relatively slower combustion front propagation and anticipated extinction during CFQ experiments under low-gravity conditions find for the first time in this work a reasonable justification. It is also worth mentioning that this conclusion holds true independently from the mode (top or bottom) sample ignition.

It should be noted that we have confined the analysis earlier to systems characterized by relatively small porosity changes during reaction. On the other hand, the formation of high-porosity (greater than about 60%) within the reacting sample provides an increase of the contribution to heat transfer by radiation in addition to the thermal conduction, which conversely prevails for lower porosity.[20] Unfortunately, direct experimental investigations on pellet expansion during combustion synthesis processes have been performed only for systems showing remarkable sample elongations (greater than about 50%) during reaction.[10,11,13,15] For these specific systems, in fact, the effect of gravity on combustion front velocity cannot be established as a general statement,[10] probably due to the opposite effect of porosity on radiation and thermal conduction.

In addition, as reported previously, natural convection in the liquid phase occurring at macroscopic scale (reaction zone) may significantly contribute to the overall heat transport. Even if specific investigations on the effect of natural convection occurring in the liquid phase are not available in the literature, it follows that this heat-transfer mechanism may affect the apparent thermal conductivity of the reaction zone. In particular, for the case of ignition from the sample bottom-side under terrestrial conditions, natural convection in the layer A (cf. Figure 12) increases the net heat flux from the reaction zone to the unreacted part of the pellet. As a consequence, the apparent thermal conductivity, k_{mix}, is expected to increase. On the contrary, for the case of ignition from the sample top side, natural convection occurring in the layer B (cf. Figure 12) is likely to results in a decrease of k_{mix}. Consequently, *natural convection in the liquid phase represents a reasonable justification of the general experimental evidence that U_C is found higher for the case of ignition from the bottom with respect to the case of ignition from the top*.

Effect of gravity on product microstructure

As summarized in Figure 10, product grain evolution during combustion synthesis processes involves several phenomena, which determine grain size and phase distribution in the final products. Among these, crystallization (nucleation and grain growth), and Ostwald ripening (also known as contactless coalescence or coarsening) depend on temperature and concentration distributions at the microscopic (particle) scale. On the other hand, coalescence and phase separation are influenced by the relative motion (mass transport) between settling or buoyancy of the forming product particles/grains within a molten phase.

However, on the basis of the results previously reported, natural convection and single particle movement**,** do not contribute appreciably to heat and mass-transfer coefficients. Therefore, *nucleation, grain growth and Ostwald ripening are not expected to be responsible for the relatively coarser product microstructure obtained under terrestrial g-level*. Regarding this aspect, a completely different conclusion was drawn by other authors who adopted the thickness of the molten layer as characteristic length for heat and mass transfer-controlled phenomena involved during microstructural formation.[10,21,24] In this authors' view, this choice is not appropriate, being, as proposed in this work, the length-scale of such phenomena summarized above the particle size.

The effect of gravity on relative particle motion, which may lead to coalescence and phase segregation phenomena, is then examined in what follows.

Effect of gravity on product grain size through coalescence

Under the action of the driving force given by the different density between liquid phase and solid particles, the latter may coalesce if they come into contact during their motion. Specifically, this phenomenon we expect to take place if the molten

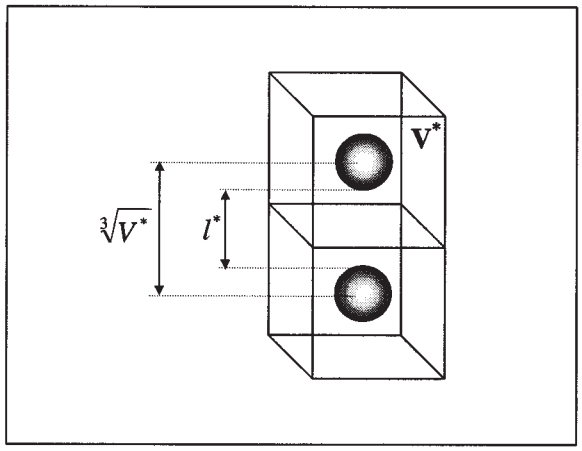

Figure 13. Evaluation of the characteristic distance between solid particles.

layer lifetime, ($t_m = t_{m,(A)} + t_{m,(B)}$, cf. Figure 12) is greater than the time needed for coalescence occurrence, that is

$$t_m > t_t + t_c \tag{30}$$

where t_t is the time spent by a traveling (settling/buoyancing) particle to reach another one, and t_c is the time interval required for two separate contacting particles to merge into a single one.

By assuming the solution-reprecipitation as coalescence mechanism[53], t_c can be evaluated as follows[54]

$$t_c = \frac{k_B T}{D_m \Omega \gamma_{sl}} d_p^3 \tag{31}$$

where γ_{sl} is the interfacial energy between liquid phase and solid particles undergoing coalescence, D_m and Ω represent diffusion coefficient in the liquid phase and atomic volume of the mobile species, respectively. It is seen from Eq. 31 that t_c is not gravity dependent.

Conversely, t_t can be obtained as the ratio between the average distance among solid particles, (l^*), and the particle velocity. Specifically, we propose to estimate l^* through the following equation

$$l^* = \left(\sqrt[3]{\frac{\pi}{6\phi_{(s)}}} - 1 \right) d_p \tag{32}$$

which takes into account the average particle diameter and the solid phase volume fraction ($\phi_{(s)}$). As depicted in Figure 13, Eq. 32 is obtained by assuming a simple cubic arrangement for particles which undergo coalescence. The volume available for each particle to move (V^*) is determined dividing the total volume by the number of particles. The latter quantity is the ratio between the total volume occupied by the solid phase, and the volume of each particle. It should be noted that $l^* = 0$ for $\phi_{(s)} = 0.524$, which correspond to a porosity equal to 0.476, that is the minimum porosity achievable when spherical nondeformable particles are packed in a simple cubic cell.

Solid particles travel according to both Brownian and Stokes motion. Brownian velocity can be determined through the following equation[55]

$$v_b = \sqrt{\frac{k_B T}{3\pi \mu_{(liq)} d_p t_m}} \tag{33}$$

while the terminal (Stokes) velocity has been already given by Eq. 8. It should be noted that, since brownian motion is gravity-independent, in order to have a considerable effect of gravity on particles motion, Stokes motion must prevail.

Three numerical examples aimed to evaluate the effect of gravity on coalescence are reported in Table 11. They all refer to systems experimentally studied in the literature under low- and terrestrial gravity conditions.[9,14,56] It may be clearly seen that relatively larger solid particles move predominantly under the action of Stokes motion and also that condition (Eq. 30) can be satisfied during the course of microstructure evolution. Hence, it is likely that *the formation of typical coarser product grain size experimentally observed when operating under 1g conditions with respect to low-g ones are due to the buoyancy/settling enhanced coalescence*.

Effect of gravity on phase separation

Let us now consider the possible effect of gravity on homogeneity (phases distribution) in combustion synthesized products. When solid and molten phases coexist or immiscible liquid phases with different densities are formed during the SHS process, gravity can induce settling or buoyancy of solid particles or/and liquid droplets, thus, enhancing phase separation. The relative importance of this phenomenon can be quantitatively estimated by defining a characteristic time of phase separation (t_{ps}) as follows

$$t_{ps} = \frac{l_{ps}}{v_p} \tag{34}$$

where l_{ps} is the corresponding characteristic length, while v_p is the velocity of the solid particle or the liquid droplet that undergoes settling or buoyancy. In order to have a significant effect on product microstructure due to phase separation, t_{ps} should be lower than the existence time of liquid phase t_m.

The choice of the characteristic length for phase separation (l_{ps}) deserves additional comments, since it determines the length scale at which the effect of phase segregation is manifested. Specifically, macrosegregation can be quantitatively evaluated by adopting as characteristic length the height of the molten layer formed during the combustion process. In this case, a conservative estimate of l_{ps} is 110^{-3} m. On the other hand, when microsegregation (which occurs at the particle scale) is considered, l_{ps} can be chosen equal to the characteristic distance between particles undergoing phase separation (cf. Eq. 32).

When evaluating the characteristic time for macrosegregation (cf. Eq. 34), possible interactions during particle motion (hindered settling/buoyancing) should be taken into account. Accordingly, v_p may be estimated through the following relationship[39]

Table 11. Parameters to Evaluate Solid Particles Coalescence and Phase Separation

System Investigated	HfB_2 + 70 Vol% Al[14]	TiB_2 + 70 Vol% Ni_3Ti[56]	TiB_2 + 60 wt% Ni_3Al[9]	Ref.
T [K]	1349	1569	1937	(*)
$\rho_{(s)}$ *[kg m^{-3}]*	11200	4520	4520	[30]
	Al 2248		*Al* 2065	[36]
$\rho_{liq)}$ *[kg m^{-3}]*		*Ni* 7976	*Ni* 7728	[43]
		Ti 4398		[40]
		Mix 6795	*Mix* 5664	Eq. 9
$\mu_{(liq)}$ *[Pa s]*	*Al* $6.49\ 10^{-4}$		*Al* $4.15\ 10^{-4}$	[37]
		Ni $7.79\ 10^{-3}$	*Ni* $3.75\ 10^{-3}$	[37]
		Ti $6.25\ 10^{-3}$		[37]
		Mix $7.41\ 10^{-3}$	*Mix* $2.91\ 10^{-3}$	Eq. 9
R_a *[nm]*	*Hf* 0.159		*Ti* 0.147	[30]
		B 0.097		
D_m *[m^2/s]*	$1.26\ 10^{-9}$	$1.33\ 10^{-9}$	$4.17\ 10^{-9}$	(**)
d_p *[μm]*	0.4	0.3–2.3	1–3	—
t_m *[s]*	55	12	9.1	—
t_c *[s]*	$1.07\ 10^{-2}$	$5.79\ 10^{-2}$–26.1	0.844–22.8	(***)
ν_t *[μm/s]*	1.20	$1.51\ 10^{-2}$–0.885	0.214–1.93	this work
ν_b *[μm/s]*	0.372	0.106–0.293	0.189–0.327	this work
Ratio ν_t/ν_b	3.23	$5.13\ 10^{-2}$–8.35	0.654–10.2	this work
$\phi_{(s)}$	0.195	0.18	0.319	—
$l^* = l_{ps}$ *(micro) [μm]*	0.156	0.128–0.983	0.180–0.540	this work
$t_t = t_{ps}$ *(micro) [s]*	0.130	1.11–8.52	0.281–0.842	this work
ν_p *[μm/s]*	0.439	$5.98\ 10^{-3}$–0.352	$3.59\ 10^{-2}$–0.323	this work
t_{ps} *(macro) [s]*	$2.28\ 10^3$	$2.84\ 10^3$–$1.67\ 10^5$	$3.09\ 10^3$–$2.78\ 10^4$	this work

(*) $T = (T_C + T_m)/2$ where $T_m = T_{m,Al} = 933\ K$,[14] $T_m = T_{m,Ni_3Ti} = 1481\ K$,[57] $T_m = T_{m,Ni_3Al} = 1668\ K$.[9]
(**) These values have been obtained by averaging diffusivities estimated through Stokes-Einstein equation[48] for each diffusing component of the system under investigation: Hf and B (HfB_2 + 70 Vol% Al system) and Ti and B (TiB_2 + 70 Vol% Ni_3Ti and TiB_2 + 60 wt% Ni_3Al systems).
(***)In Eq. 31 it has been assumed $\gamma_{sl} \cong 1\ J\,m^{-2}$ for each system under investigation, while the atomic volume Ω has been calculated by averaging the atomic radius of Hf and B (HfB_2 + 70 Vol% Al system) and Ti and B (TiB_2 + 70 Vol% Ni_3Ti and TiB_2 + 60 wt% Ni_3Al systems).

$$\nu_p = \nu_t(1 - \phi_{(s)})^{4.65} \tag{35}$$

where the terminal velocity ν_t is evaluated through Eq. 8. Conversely, when considering phase distribution at the microscopic scale (microsegregation), ν_p is assumed equal to ν_t, so that t_{ps} is equal to t_t.

It is clearly seen from Table 11 that the characteristic time of macrosegregation is much higher than the existence time of liquid phase, while the characteristic time of microsegregation results lower than t_m for all the systems investigated. Therefore, macrosegregation of product particles is not expected to be significant during combustion synthesis processes, whereas phase separation at the particle scale may play a significant role during products microstructure formation under terrestrial gravity conditions. As a consequence, *microsegregation is likely to be responsible of the relatively less homogeneous microstructure observed under terrestrial conditions as compared to that obtained under reduced gravity environment.*

Concluding Remarks

The results of the self-propagating combustion synthesis of titanium diboride/titanium aluminides composites performed during parabolic flight experiments are reported and discussed in this work. Regardless of the gravitational conditions (low-gravity or terrestrial), it is found that combustion wave velocity and temperature decrease as the aluminide/diboride ratio is augmented due to the corresponding decrease of system exothermicity.

When the reaction is performed under reduced gravity conditions, combustion front proceeded slower as compared to experiments conducted on the ground. Accordingly, combustion front quenching experiments revealed that extinction of combustion wave occurred earlier in low-gravity environment. On the other hand, no remarkable changes in combustion temperature are seen. These results are found consistent with the most important experimental outcomes reported in the literature on this field and summarized also in this article.

In order to explain these experimental observations, a theoretical analysis of possible heat and mass transport gravity-dependent phenomena taking place during combustion synthesis is carried out by means of appropriate dimensionless numbers.

It is found that natural convection within the gas phase has a negligible effect in comparison to radiation on heat loss from the external surface of the reacting pellet to the surroundings. This finding, in addition to the fact that the rate of heat released by chemical reaction is found to be insensitive to *g*-level, indicates that gravity is not expected to substantially affect combustion temperature, which is in agreement with experimental evidence.

Vice versa, it is seen that even small sample porosity variations due to pellet expansion are expected to play an important role by influencing heat transfer (that is, apparent thermal conductivity) inside the reaction zone. This aspect justifies the relatively slower combustion front and earlier quenching extinction when reaction is performed under reduced gravity conditions.

Moreover, free convection taking place in the molten phase during combustion synthesis process is expected to represent a reasonable justification of the general experimental evidence that under terrestrial conditions combustion front velocity is

relatively higher for the case of ignition from the bottom, with respect to the case of ignition from the top.

In addition, coalescence of product solid particles may be considered responsible for the relatively coarser microstructure typically observed under terrestrial conditions, as compared to that obtained under low-gravity, while microsegregation is likely to contribute to homogeneity.

Acknowledgments

The financial support of Agenzia Spaziale Italiana (ASI), Belgian Federal Office for Scientific, Technical and Cultural affairs (OSTC) and European Space Agency (ESA) is gratefully acknowledged. We also acknowledge one anonymous reviewer for his fruitful comments.

Notation

Bi = biot number
Bo = bond number
C_p = heat capacity, $J\ kg^{-1}\ K^{-1}$
d_p = particle/droplet/bubble diameter, m;
D_m = diffusion coefficient, $m^2\ s^{-1}$
E = activation energy, $J\ mol^{-1}$
g = gravity acceleration, $m\ s^{-2}$
Gr_H = heat Grashof number
Gr_M = mass Grashof number
h = heat-transfer coefficient, $W\ m^{-2}\ K^{-1}$
k = thermal conductivity, $W\ m^{-1}\ K^{-1}$
k_B = Boltzmann constant, $J\ K^{-1}$
k_m = mass-transfer coefficient, $m\ s^{-1}$
k_{mix} = apparent thermal conductivity of the reacting mixture, $W\ m^{-1}\ K^{-1}$
k_0 = pre-exponential factor for chemical reaction, s^{-1}
k_x = thermal conductivity of solid porous matrix, $W\ m^{-1}\ K^{-1}$
K = porous medium permeability, m^2
l^* = microscopic characteristic length, m
l_{ps} = characteristic length of phase separation, m
L = pellet length, m
L^* = macroscopic characteristic length, m
Ma_H = heat Marangoni number
Ma_M = mass Marangoni number
Nu = Nusselt number
P = gas pressure, MPa
Pe_H = heat Peclet number
Pr = Prandtl number
R = universal gas constant, $J\ mol^{-1}\ K^{-1}$
R_a = atomic radis, nm
Ra = Rayleigh number
Ra^* = critical Rayleigh number
Re_p = Reynolds particle number
Sc = Schmidt number
Sh = Sherwood number
St = Stefan number
t_c = characteristic time of coalescence, s
t_m = existence time of liquid phase, s
$t_{m,(A)}$ = existence time of liquid phase in the layer A, s
$t_{m,(B)}$ = existence time of liquid phase in the layer B, s
t_{ps} = characteristic time of phase separation, s
t_t = characteristic time for particles to come into contact, s
T = temperature, K
T_m = melting temperature, K
$T_{m,(A)}$ = melting temperature of the low-melting component in the layer A, K
$T_{m,(B)}$ = melting temperature of the low-melting component in the layer B, K
T_C = combustion temperature, K
T_0 = ambient temperature, K;
x = intermetallic/boride molar ratio
U_C = combustion front velocity, $m\ s^{-1}$
v_b = brownian velocity, $m\ s^{-1}$
v_p = particle velocity, $m\ s^{-1}$
v_t = terminal (Stokes) velocity, $m\ s^{-1}$
V^* = volume available for each particle to move, m^3
z = axial direction, m

Greek letters

β = thermal expansion coefficient, K^{-1}
$\chi_{i,(j)}$ = molar fraction of the component i in the phase j
ΔH_R = heat of reaction, $J\ kg^{-1}$
ΔL = pellet elongation, %
$\Delta\rho$ = density difference, $kg\ m^{-3}$
ΔT = temperature difference, K
ε = porosity
ϕ = volume fraction
$\phi_{i,(j)}$ = volume fraction of component i in the phase j
γ_{lv} = liquid/vapor interfacial energy, $J\ m^{-2}$
γ_{sl} = solid/liquid interfacial energy, $J\ m^{-2}$
λ = parameter appearing in Eq. 5
μ = viscosity, $Pa\ s$
ρ = density, $kg\ m^{-3}$
ρ_0 = initial density of reacting sample, $kg\ m^{-3}$
σ = Stefan-Boltzmann constant, $W\ m^{-2}\ K^{-4}$
$\omega_{i,(j)}$ = mass fraction of the component i in the phase j
Ω = atomic volume, m^3

Subscripts

Al = aluminum
Ar = argon
B = boron
(c) = continuous phase
(d) = dispersed phase
(f) = fluid phase
mix = mixture
(gas) = gas phase
Hf = hafnium
(liq) = liquid phase
Ni = nickel
Ni_3Al = nickel aluminum intermetallic compound
Ni_3Ti = nickel titanium intermetallic compound
(s) = solid phase
Ti = titanium
TiB_2 = titanium diboride

Literature Cited

1. Merzhanov AG, Borovinskaya IP. Self-propagated high-temperature synthesis of refractory inorganic compounds. *Dokl Akad Nauk*. 1972; 204:366.
2. Munir ZA, Anselmi-Tamburini U. Self-propagating exothermic reactions: the synthesis of high-temperature materials by combustion. *Mater Sci Rept.* 1989;3:277.
3. Merzhanov AG. History and recent developments in SHS. *Ceram Int.* 1995;21:371.
4. Hlavacek V, Puszynski JA. Chemical engineering aspects of advanced materials. *Ind. Eng Chem Res.* 1996;35:349.
5. Varma A, Rogachev AS, Mukasyan AS, Hwang S. Combustion synthesis of advanced materials: Principles and applications. *Adv Chem Eng.* 1998;24:79.
6. Shteinberg AS, Scherbakov VA, Martynov VV, Mukhoyan MZ, Merzhanov AG. Self-propagating High-temperature synthesis of high-porosity materials under zero-g conditions. *Dokl Akad Nauk SSSR*. 1991;318:337.
7. Odawara O, Mori K, Tanji A, Yoda S. Thermite reaction in a short microgravity environment. *J Mater Synth. Proc.* 1993;1:203.
8. Hunter KR, Moore JJ. The effect of gravity on the combustion synthesis of ceramic and ceramic-metal composites. *J Mater Synth Proc.* 1994;2:355.
9. Yi HC, Varma A, Rogachev AS, McGinn PJ. Gravity-induced microstructural nonuniformities during combustion synthesis of intermetallic-ceramic composite materials. *Ind Eng Chem Res.* 1996;35:2982.
10. Mukasyan A, Pelekh A, Varma A, Rogachev A. Effects of gravity on combustion synthesis in heterogeneous gasless systems. *AIAA J*. 1997; 25:1821.

11. Mukasyan AS, Pelekh A, Varma A. Combustion synthesis in gasless systems under microgravity conditions. *J Mater Synth Proc.* 1997;5: 391.
12. Odawara O. Microgravitational combustion synthesis. *Ceram. Int.*, 3, 273, (1997).
13. Merzhanov AG, Rogachev AS, Sanin VN, Scherbakov VA, Sytschev AE, Yukhvid VI. Self-propagating high-temperature synthesis (SHS) under microgravity. *Joint I Pan-Pacific basin workshop and IV Japan-China Workshop on Microgravity*, H. Azuma ed. The Japan Society of Microgravity Application. 1998:119.
14. Yi HC, Woodger TC, Moore JJ, Guignè JY. The effect of gravity on the combustion synthesis of metal-ceramic composites. *Metall Mater Trans B*. 1998;29:889.
15. Tanabe Y, Sakamoto T, Okada N, Akatsu T, Yasuda E, Takasu S, Sabato T. Effect of gravity on Titanium Carbide foams by Self-propagating High-temperature Synthesis. *J. Mater. Res.*, 14, 1516, (1999).
16. Merzhanov AG, Sanin VN, Yukhvid VI. On peculiarities of structure formation in combustion of high-caloric metallothermic compounds under microgravity conditions. *Dokl Phys.* 2000;45:38.
17. Axelbaum RL, Moore JJ. *Microgravity Combustion*, *Fire In Fall*. Howard D. Ross; 2001.
18. Medda E, Orrù R, Cao G, Fry J, Guignè JY, Zell M. Effects of Microgravity on High-Temperature Self-Propagating Reactions. *Proc. 1st Int. Symposium On Microgravity Research In Physical Sciences And Biotechnology*, Esa Sp-2001;454:299.
19. Merzhanov AG, Rogachev AS, Rumanov EN, Sanin VN, Sytschev AE, Scherbakov VA, Yukhvid VI. Influence of microgravity on self-propagating high-temperature synthesis of refractory inorganic compounds. *Cosmic Res.* 2001;39:210.
20. Mukasyan AS, Lau C, Varma A. Gasless combustion of aluminum particles clad by nickel. *Combust Sci and Tech.* 2001;170:67.
21. Lau C, Mukasyan A, Pelekh A, Varma A. Mechanistic studies in combustion synthesis of NiAl-TiB_2 composites: Effects of gravity. *J Mater Res.* 2001;16:1614.
22. Merzhanov AG. SHS processes in microgravity activities: first experiments in space. *Adv. Space Res.*, 29, 487, (2002).
23. Castillo M, Moore JJ, Schowengerdt FD, Ayers RA, Zhang X, Umakoshi M, Yi HC, Guigne JY. Effects of gravity on combustion synthesis of functionally graded materials. *Adv Space Res.* 2003;32(2): 265.
24. Mukasyan A, Lau C, Varma A. Influence of gravity on combustion synthesis of advanced materials. *AIAA J.* 2005;43:225.
25. Locci AM, Orrù R, Cincotti A, Licheri R, Cao G. Remarks on Gravity-Driven Transport Phenomena during Combustion Synthesis Processes, *ELGRA Biennial Meeting and General Assembly* Santorini, Greece: September 21st-23rd, 2005.
26. Cincotti A, Licheri R, Locci AM, Orrù R, Cao G. Combustion Synthesis of novel materials: experimental and modeling. *J Chem Technol Biotechnol.* 2003;78(2-3):122.
27. Orrù R, Cao G, Munir ZA. Field-Activated Combustion Synthesis of Titanium Aluminides. *Metall Mater Trans. A.* 1999;30:1101.
28. Nield DA, Bejan A. *Convection in porous media*. 2nd ed., Springer; 1999.
29. Reid RC, Prausnitz JM, Poling BE. The properties of gases and liquids, 4th ed., McGraw-Hill; 1988.
30. *CRC, Materials Science and Engineering Handbook*. 3rd ed., CRC Press LLC; 2001.
31. Barin I. *Thermochemical data of pure substances*. VCH; 1993.
32. Gonzo EE. Estimating correlations for the effective thermal conductivity of granular materials. *Chem Eng J.* 2002;90:299.
33. Kaviany M. *Principles of heat transfer in porous media*. Springer-Verlag; 1995.
34. Ishikawa T, Paradis PF, Itami T, Yoda S. Non-contact thermophysical property measurements of refractory metals using an electrostatic levitator. *Meas Sci Technol.* 2005;16:443.
35. Bird RB, Steward WE, Lightfoot EN. *Transport Phenomena*. John Wiley & Sons; 1960.
36. Assael MJ, Kakosimos K, Banish RM, Brillo J, Egry I, Brooks R, Quested PN, Mills KC, Nagashima A, Sato Y, Wakeham WA. Reference data for the density and viscosity of liquid aluminum and liquid iron. *J Phys Chem Ref Data*. 2006;35(1):285.
37. Battezzati L, Greer AL. The viscosity of liquid metals and alloys. *Acta metal.* 1989;37:1791.
38. Mills KC, Monaghan BJ, Keene BJ. Thermal conductivities of molten metals: Part 1 Pure metals. *Int Mater Rev.* 1996;41:209.
39. Perry RH, Green D. *Perry's chemical engineering handbook*, 6th ed., McGraw-Hill; 1984.
40. Paradis PF, Rhim WK. Non-contact measurements of thermophysical properties of titanium at high temperature. *J Chem Thermodyn.* 2000; 32:123-133.
41. Viswanath DS, Mathur BC. Thermal conductivity of liquid metals and alloys. *Metall. Trans.* A 1972;3:1769.
42. Turner JS. *Buoyancy effects in fluids*. Cambridge University Press; 1979.
43. Chung SK, Thiessen DB, Rhim WK. A non contact measurement technique for the density of solid and liquid materials. *Rev Sci Instrum.* 1996;67(9):3175.
44. Treybal RE. *Mass transfer operations*. McGraw-Hill; 1985.
45. Cowley SJ, Davis SH. Viscous thermocapillary convection at high Marangoni number. *J Fluid Mech.* 1983;135:175.
46. Molenkamp T. Marangoni convection, mass transfer and microgravity. *Rijksuniversiteit Groningen.* The Netherlands; 1998. MSc Thesis.
47. Melissari B, Argyropoulos SA. Development of a heat transfer dimensionless correlation for spheres immersed in a wide range of Prandtl number fluids. *Int J Heat Mass Transfer*. 2005;28:4333.
48. Geiger GH, Poirer DR. *Transport phenomena in metallurgy*, Addison-Wesley Pub. Co; 1973.
49. Middleman S. *An introduction to mass and heat transfer: principles of analysis and design*. John Wiley & Sons; 1998.
50. Merzhanov AG, Khaikin BI. Theory of combustion waves in homogeneous media. *Prog. Energy Combust Sci.* 1988;14:1.
51. Makino A. Fundamental aspects of the heterogeneous flame in the self-propagating high-temperature synthesis (SHS) process. *Prog Energy Combust. Sci*. 2001;27:1.
52. Paradis PF, Ishikawa T, Yoda S. Non-contact density measurements of liquid, undercooled, and high temperature solid boron. *Appl Phys Lett.* 2005;86(15):1.
53. German RM. *Sintering theory and practice*. John Wiley & Sons; 1996.
54. Kingery WD, Bowen HK, Uhlmann DR. *Introduction to ceramics* 2nd ed.; John Wiley & Sons; 1976.
55. Nelson E. *Dynamical Theories of Brownian Motion*. Princeton University Press; 1967.
56. Yi HC, Woodger TC, Moore JJ, Guignè JY. Combustion characteristic of the Ni_3Ti-TiB_2 intermetallic matrix composites. *Metall Mater Trans B*. 1998;29:867.

Manuscript received Apr. 21, 2006, and revision received Aug. 8, 2006.